

Effects of anisotropy in spin molecular-orbital coupling on effective spin models of trinuclear organometallic complexes

J. Merino

*Departamento de Física Teórica de la Materia Condensada,
Condensed Matter Physics Center (IFIMAC) and Instituto Nicolás Cabrera,
Universidad Autónoma de Madrid, Madrid 28049, Spain*

A. C. Jacko, A. L. Khosla and B. J. Powell

*Centre for Organic Photonics and Electronics, School of Mathematics and Physics,
The University of Queensland, Brisbane, Queensland 4072, Australia*

(Dated: October 4, 2018)

We consider the magnetic properties of trinuclear coordinated organometallic complexes in which Coulomb interactions and spin molecular-orbital coupling are relevant. The $\text{Mo}_3\text{S}_7(\text{dmit})_3$ crystals considered here consist of two-dimensional layers of decorated honeycomb lattices. Pseudospin-1 moments localized on the organometallic clusters under a trigonal splitting emerge from the interplay of Coulomb repulsion and spin molecular-orbital coupling. We explore the possible realization of a Kitaev-type spin model within a single honeycomb layer, studying the dependence of spin exchange anisotropies on the underlying microscopic parameters. We elucidate the crucial role played by intralayer spin exchange to produce magnetic anisotropies between the pseudospins in the presence of spin molecular-orbital coupling. In contrast to, say, transition metal oxides the intrinsic non-spherical symmetry of the clusters constituting multinuclear coordinated complexes can lead to very different transverse and longitudinal spin molecular-orbital couplings which directly influence the magnetic anisotropies and trigonal splittings. Our analysis shows how the spin molecular-orbital anisotropies found in $\text{Mo}_3\text{S}_7(\text{dmit})_3$ greatly enhance trigonal splittings in comparison with isotropic couplings. However, we find that these enhancements are not sufficient to destroy the Haldane phase in $\text{Mo}_3\text{S}_7(\text{dmit})_3$ and drive the crystal into a topologically trivial phase. We predict a quantum phase transition from a Haldane phase to a magnetically ordered phase at sufficiently strong external magnetic fields.

PACS numbers: 71.30.+h; 71.27.+a; 71.10.Fd, 75.10.Kt

I. INTRODUCTION

The interplay of strong Coulomb interaction and spin-orbit coupling (SOC) can lead to emergent quantum phases¹ and new phenomena which remain poorly understood. The conventional Mott transition can be strongly affected by SOC leading to a topological Mott insulator with bulk charge gap but fractionalized surface states carrying spin but no charge². Such states may be realized in Ir-based transition metal oxides such as Sr_2IrO_4 . In contrast to conventional Mott insulators, the spin exchange interactions arising in Mott insulators with SOC are typically anisotropic so that the effective magnetic model is a quantum compass³ model instead of the conventional Heisenberg model. A possible realization of a quantum compass model on a hexagonal lattice, *i. e.* a Heisenberg-Kitaev model^{4–6} may be found in Na_2IrO_3 and Li_2IrO_3 materials in which SOC removes the orbital degeneracy of the 5d electrons leading to effective $S = 1/2$ pseudospins. Metal-organic frameworks may provide an alternative realization of Kitaev's honeycomb spin model⁷. Interestingly, the Kitaev model is exactly solvable: it sustains a spin liquid ground state whose low energy excitations are Majorana fermions⁸. In other iridates with strong SOC such as Sr_2IrO_4 , an antisymmetric Dzyaloshinski-Moriya (DM) interaction arises associated with the lack of an inversion symmetry center.

Multinuclear coordinated organometallic complexes are strongly correlated materials in which spin-orbit coupling is relevant^{9–11}. The elementary building blocks of these materials are molecular clusters containing transition metal ions whose d-orbitals are hybridized with molecular orbitals where each of the hybrids is adequately described through a single Wannier orbital¹². The coupling of the spin with the electron currents around the Wannier orbitals describing each molecule gives rise to a spin molecular-orbital coupling (SMOC)^{9,10}. In $\text{Mo}_3\text{S}_7(\text{dmit})_3$, honeycomb networks of $\text{Mo}_3\text{S}_7(\text{dmit})_3$ molecules are stacked on top of each other along the c -direction of the crystal.

Since $\text{Mo}_3\text{S}_7(\text{dmit})_3$ molecules can be described by three Wannier orbitals¹², the layers consist of decorated honeycomb lattices as shown in Fig. 1. The electronic and magnetic properties of the decorated honeycomb lattice are interesting both in the weakly and strongly interacting limit. At weak coupling, a tight-binding model on such lattice leads to topological insulating phases when SOC is turned on which display the quantum spin hall (QSH) effect¹³ as predicted in graphene¹⁴. Since at strong coupling, the exact ground state of the Kitaev-Heisenberg model on the decorated honeycomb lattice¹⁵, is a exotic chiral spin liquid (CSL), it is interesting to find possible realizations of the decorated honeycomb lattice in actual materials probing their rich physics.

Organometallic complexes have intrinsic structural properties which make them different to transition metal oxides. A crucial difference comes from the fact that isolated molecular clusters break the spherical symmetry present in isolated transition metal ions. While the total angular momentum of the ion, J , is conserved, it is only the component perpendicular to the molecular plane, J_z , that is conserved in cyclic molecular clusters. Hence, in these systems, anisotropies are intrinsic to the molecules constituting the material, whereas in transition metal oxides anisotropies can only be achieved via the environment surrounding the ions in the crystal. This suggests that anisotropic spin exchange interactions may be easily generated in organometallic complexes due their intrinsic structure. These anisotropies may be further enhanced by the anisotropic SMOC typically found in these systems.^{10,16} SMOC is an emergent coupling between electron currents circulating around the cyclic molecules and the electron spin. Also by tuning the relative orientation between molecules in the crystal a Dzyaloshinskii-Moriya interaction can be generated¹⁶. All the above has suggested that these materials are ideal playgrounds for the realization of quantum compass models³ such as the Kitaev model.

In our recent work^{11,16} we have derived an effective super-exchange hamiltonian that captures the magnetic properties of trinuclear coordinated complexes at strong coupling. The combination of onsite Coulomb repulsion, U , and SMOC, λ , was found to lead to pseudospin-one moments localized at each triangular cluster under the influence of a trigonal splitting, D . The pseudospins were found to be arranged in weakly coupled chains due to the special lattice structure of trinuclear organometallic complexes.^{11,16} The lattice structure is such that three hopping amplitudes connect two nearest-neighbor molecules along the c -direction while only one hopping amplitude connects nearest-neighbor molecules in the $a-b$ planes, cf. Fig. 3. As U is increased exchange of electrons between nearest-neighbor molecules in the $a-b$ plane is suppressed as compared to exchange between molecules along the c -direction. This leads to a quasi-one-dimensional effective spin exchange model.¹⁶

The aim of our present work is twofold: to understand the role played by the different microscopic parameters in generating spin exchange anisotropies in these crystals and to describe our general method developed for obtaining spin exchange couplings in trinuclear organometallic complexes. More specifically, we analyze the role played by the interplay of Coulomb repulsion and intracluster exchange in producing anisotropic exchange couplings. We also study the effect of SMOC anisotropy, $\lambda_{xy} \neq \lambda_z$, present in these systems that was not considered in our previous work¹¹. We specifically search for the possibility of realizing Kitaev-type spin models in the decorated honeycomb lattices of Fig. 1 which might be obtained by isolating single layers of the $a-b$ planes of $\text{Mo}_3\text{S}_7(\text{dmit})_3$ crystals. We find that the effective exchange couplings between neighbor triangular clusters are anisotropic *only*

when *both* SMOC *and* intracluster exchange, J_F , are present. We explicitly show how cluster models which only consider an onsite U , lead to the conventional antiferromagnetic Heisenberg model for pseudospin-1 in the honeycomb lattice. We explore the effect of anisotropic SMOC, $\lambda_{xy} \neq \lambda_z$, finding that the largest anisotropic spin exchange couplings and trigonal splittings emerge for $\lambda_{xy}/\lambda_z < 1$, which is the parameter regime realized in $\text{Mo}_3\text{S}_7(\text{dmit})_3$. Based on *ab initio* estimates of SMOC¹⁰, which suggest that $\lambda_{xy} \approx \lambda_z/2$, we conclude that trigonal splittings are smaller than the exchange couplings along the c -direction, $D < J^c$, so that the Haldane phase is the ground state rather than the topologically trivial D -phase, *i. e.* the tensor product of the $j = 0$ singlets (where j is the z -component of the total angular momentum) at each cluster, which is expected for $D > J^c$. We predict that under a sufficiently large external magnetic field, the Haldane phase can be destroyed giving way to a three-dimensional ordered magnet. This occurs at a critical magnetic field, $h_c \sim \Delta_s$, where Δ_s is the zero-field Haldane gap of the $S = 1$ chain.

The present paper is organized as follows. In Section II we introduce the minimal strongly correlated model for describing the electronic properties of isolated triangular $\text{Mo}_3\text{S}_7(\text{dmit})_3$ molecules in the presence of SMOC. In Section III we analyze the electronic structure of two coupled trimers arranged as two nearest-neighbor molecules in the $a-b$ plane and also as two nearest-neighbor molecules along the c -direction. The energy level spectra of two coupled trimers is obtained exactly and compared to second order perturbation theory. In section IV, the combination of the numerical perturbative approach with an analytical canonical transformation, used to extract the exchange interactions between the nearest neighbor pseudospins, is introduced and explained in detail. In section V, we discuss the qualitative phase diagram expected for the quasi-one-dimensional spin model arising from our approach. Finally, in section VI, we conclude providing an outlook of our work.

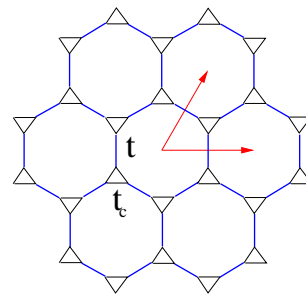


FIG. 1: The decorated honeycomb lattice realized in the $a-b$ planes of $\text{Mo}_3\text{S}_7(\text{dmit})_3$ crystals. The small triangles represent the organometallic triangular $\text{Mo}_3\text{S}_7(\text{dmit})_3$ molecules located at sites of the honeycomb lattice. The intracluster hopping, t_c and the intercluster hopping t entering our model (1) are also shown.

II. MODEL OF ISOLATED TRIMERS IN THE PRESENCE OF SMOC

The triangular $\text{Mo}_3\text{S}_7(\text{dmit})_3$ molecules are the building blocks of these crystals. In order to understand the SMOC effects on the electronic and magnetic properties of these systems we first discuss the relevant model for isolated triangular clusters. The simplest strongly correlated model is a Hubbard model on a triangle in the presence of SMOC^{12,17,18}:

$$H = H_0 + H_{\text{SMOC}} + H_{U-J_F}. \quad (1)$$

The non-interacting part reads

$$H_0 = -t_c \sum_{\langle ij \rangle \sigma} \left(a_{i\sigma}^\dagger a_{j\sigma} + H.c. \right), \quad (2)$$

where t_c is the hopping between nearest-neighbor sites in the cluster and $c_{i\sigma}^\dagger$ creates an electron at site i with spin σ . The general SMOC contribution is⁹

$$\begin{aligned} H_{\text{SMOC}} &= \lambda_{xy}(L_x S_x + L_y S_y) + \lambda_z L_z S_z \\ &= \lambda_{xy} \left(\frac{L^+ S^- + L^- S^+}{2} \right) + \lambda_z L_z S_z, \end{aligned} \quad (3)$$

where L is the molecular orbital angular momentum and \mathbf{S} the total spin of electrons in the cluster. λ_{xy} describes the transversal SMOC while λ_z describes the longitudinal contribution.

Finally, the Hubbard-Heisenberg term reads

$$H_{U-J_F} = U \sum_i n_{i\uparrow} n_{i\downarrow} + J_F \sum_{\langle ij \rangle} \left(\mathbf{S}_i \cdot \mathbf{S}_j - \frac{n_i n_j}{4} \right), \quad (4)$$

where U is the onsite Hubbard interaction and J_F is an intracuster exchange interaction and $n_{i\sigma} = a_{i\sigma}^\dagger a_{i\sigma}$, the number operator. The non-interacting part (2) can be readily diagonalized:

$$H_0 = \sum_{k\sigma} \epsilon_k b_{k\sigma}^\dagger b_{k\sigma}, \quad (5)$$

using Bloch operators:

$$b_{k\sigma}^\dagger = \frac{1}{\sqrt{3}} \sum_{j=1}^3 e^{ik\phi(j-1)} a_{j\sigma}^\dagger, \quad (6)$$

with $\phi = \frac{2\pi}{3}$. So $k = 0, \pm 1$ correspond to the allowed $0, \pm \frac{2\pi}{3}$ momenta in the first Brillouin zone of the triangular cluster with energies $\epsilon_0 = -2t_c$ and $\epsilon_{\pm 1} = \epsilon_{-1} = t_c$.

The SMOC contribution to H is most naturally described using Condon-Shortley states which are eigenstates of the z -component of the angular momentum, L_z , of the cluster^{9,19},

$$c_{k\sigma}^\dagger = \text{sgn}^k(-k) \frac{1}{\sqrt{3}} \sum_{j=1}^3 e^{ik\phi(j-1)} a_{j\sigma}^\dagger. \quad (7)$$

More explicitly we have

$$\begin{aligned} c_{0,\sigma}^\dagger &= b_{0\sigma}^\dagger \\ c_{1\sigma}^\dagger &= -b_{1,\sigma}^\dagger \\ c_{-1\sigma}^\dagger &= b_{-1,\sigma}^\dagger. \end{aligned} \quad (8)$$

Note that due to Bloch's theorem applying in the cluster, the z -component of angular momentum is defined up to $3n$ (in units of ϕ) with n an integer i . *e.* Bloch states with momentum k' satisfying $k = k' \pm 3n$ are equivalent to the $k = 0, \pm 1$ states.

Hence, the tight-binding part of the hamiltonian H_0 can be expressed either in terms of the Condon-Shortley or Bloch operators as

$$H_0 = t_c \sum_{\sigma, k=-1}^1 \cos(\phi k) c_{k\sigma}^\dagger c_{k\sigma} = t_c \sum_{\sigma, k=-1}^1 \cos(\phi k) b_{k\sigma}^\dagger b_{k\sigma}. \quad (9)$$

Similarly, the SMOC contribution to the hamiltonian of the isolated cluster in terms of the Condon-Shortley or Bloch operators reads

$$\begin{aligned} H_{\text{SMOC}} &= \frac{\lambda_{xy}}{\sqrt{2}} (c_{0\downarrow}^\dagger c_{-1\uparrow} + c_{1\downarrow}^\dagger c_{0\uparrow} + c_{0\uparrow}^\dagger c_{1\downarrow} + c_{-1\uparrow}^\dagger c_{0\downarrow}) \\ &\quad + \frac{\lambda_z}{2} (c_{1\uparrow}^\dagger c_{1\uparrow} - c_{1\downarrow}^\dagger c_{1\downarrow} - c_{-1\uparrow}^\dagger c_{-1\uparrow} + c_{-1\downarrow}^\dagger c_{-1\downarrow}) \\ &= \frac{\lambda_{xy}}{\sqrt{2}} (b_{0\downarrow}^\dagger b_{-1\uparrow} - b_{1\downarrow}^\dagger b_{0\uparrow} - b_{0\uparrow}^\dagger b_{1\downarrow} + b_{-1\uparrow}^\dagger b_{0\downarrow}) \\ &\quad + \frac{\lambda_z}{2} (b_{1\uparrow}^\dagger b_{1\uparrow} - b_{1\downarrow}^\dagger b_{1\downarrow} - b_{-1\uparrow}^\dagger b_{-1\uparrow} + b_{-1\downarrow}^\dagger b_{-1\downarrow}) \end{aligned} \quad (10)$$

We may now write H in the site basis, $|i\sigma\rangle$, using the transformation of Eq. (6) which leads to:

$$\begin{aligned}
H = & \sum_{\sigma} \left((-t_c + \sigma \lambda_z B^*) a_{1\sigma}^{\dagger} a_{2\sigma} + (-t_c + \sigma \lambda_z B) a_{1\sigma}^{\dagger} a_{3\sigma} + (-t_c + \sigma \lambda_z B^*) a_{2\sigma}^{\dagger} a_{3\sigma} + H.c \right) \\
& + \lambda_{xy} \sqrt{2} \left(A a_{1\downarrow}^{\dagger} a_{2\uparrow} + A^* a_{1\downarrow}^{\dagger} a_{3\uparrow} - A a_{2\downarrow}^{\dagger} a_{1\uparrow} + B^* a_{2\downarrow}^{\dagger} a_{3\uparrow} - A^* a_{3\downarrow}^{\dagger} a_{1\uparrow} + B a_{3\downarrow}^{\dagger} a_{2\uparrow} \right) + H.c. \\
& + U \sum_i n_{i\uparrow} n_{i\downarrow} + J_F \sum_{\langle ij \rangle} \left(\mathbf{S}_i \cdot \mathbf{S}_j - \frac{n_i n_j}{4} \right), \tag{11}
\end{aligned}$$

with $A = \frac{(e^{i\phi}-1)}{6}$, $B = \frac{i}{3} \sin(\phi)$, and $\sigma = \pm 1$.

Four-component relativistic *ab initio* calculations¹⁰ have found anisotropic spin-orbit couplings: $\lambda_{xy} \approx \lambda_z/2 > 0$, with $\lambda_{xy} = 0.042t_c$ and $t_c = 0.059$ eV. In our model we will fix $t_c > 0$ as the unit of energy and explore different values of SMOC and different λ_{xy}/λ_z ratios. Note that the electronic properties of the model are invariant under the particle-hole transformation $a_i^{\dagger} \rightarrow h_i, a_i \rightarrow h_i^{\dagger}$, where h_i^{\dagger} and h_i are hole operators together with the transformation $t_c \rightarrow -t_c$, $\lambda_{xy} \rightarrow -\lambda_{xy}$, $\lambda_z \rightarrow -\lambda_z$. The onsite Coulomb repulsion, U , in the Mo *d*-orbitals is comparable or even larger than the bandwidth of the relevant Mo₃S₇(dmit)₃ bands crossing the Fermi energy. We will assume $U = 10t_c$ as a reasonable estimate. Since the Mo₃S₇(dmit)₃ crystal is at 2/3-filling there are $N = 4$ electrons per triangu-

lar cluster in the crystal. In order to fully characterize the electronic structure of two coupled clusters through perturbation theory techniques we have analyzed triangular clusters with $N = 3, 4, 5$ electrons and the parameters $t_c, \lambda_{xy}, \lambda_z > 0$, relevant to Mo₃S₇(dmit)₃ crystals. Through the particle-hole transformation we can also obtain the electronic structure of triangular clusters with $N = 1$ ($N = 2$) electrons from the $N = 5$ ($N = 4$) solutions by switching the sign of $\lambda_{xy}, \lambda_z, t_c$.

Since $J_z = L_z + S_z$ is a conserved quantity: $[J_z, H] = 0$, it is convenient to use the (k, σ) representation instead of the site representation to classify the basis states according to their quantum number: $j = k + \sigma$. We have already expressed, $H_0 + H_{SMOC}$, in the (k, σ) basis through Eq. (9)-(10). The Hubbard-Heisenberg contribution can be expressed in the (k, σ) basis as

$$\begin{aligned}
H_{U-J_F} = & \frac{1}{3} \sum_k (U - 2J_F) n_{k\uparrow} n_{k\downarrow} + \frac{1}{3} \sum_{k, k', k \neq k'} (U - J_F \cos((k - k')\phi) - J_F) n_{k\uparrow} n_{k'\downarrow} \\
& + \frac{1}{3} \sum_{k, k', q \neq 0} (U - J_F \cos((k' - k - q)\phi) - J_F \cos(q\phi)) b_{k\uparrow}^{\dagger} b_{k'\downarrow}^{\dagger} b_{k'-q\downarrow} b_{k+q\uparrow}. \tag{12}
\end{aligned}$$

For the triangular clusters studied here $\frac{1}{3} \sum_{k, k', k \neq k'} (U - J_F \cos((k - k')\phi) - J_F) n_{k\uparrow} n_{k'\downarrow} = \frac{U - J_F/2}{3} \sum_{k, k', k \neq k'} n_{k\uparrow} n_{k'\downarrow}$. Note that while for the Hubbard-Heisenberg model the effective Coulomb repulsion between electrons is different for electrons in different orbitals, in a pure Hubbard model ($J_F = 0$), all Coulomb interactions are equal to $U/3$. This has been shown to be important for finding spin exchange anisotropies in the context of transition metal oxides^{5,20}.

Hence, the full hamiltonian can be explicitly expressed in the (k, σ) basis using the expressions for H_0 , H_{SMOC} and H_{U-J_F} in Eq. (9), (10) and (12), respectively.

In the Appendix we present results for the electronic structure of trimers with $N = 3, 4, 5$ electrons expressed in this basis. From this analysis, we conclude that isolated trimers with $N = 4$ electrons in the presence of SMOC effectively behave as pseudospin-1 localized moments. In Fig. 2 we show that under SMOC the lowest energy triplet splits into a non-degenerate singlet ($j = 0$) and a doublet ($j = \pm 1$), where j is the z -component of total angular momentum. Higher energy excitations are doublets or non-degenerate under SMOC. Note that

since we have an even number of electrons in the cluster, Kramers theorem does not apply and non-degenerate states are possible.

Hence, SMOC induces a trigonal splitting at each cluster so that the effective spin model for $N = 4$ electrons in the m -th Mo₃S₇(dmit)₃ molecule in the crystal reads

$$H_m^{\text{eff}} = D(\mathcal{S}_m^z)^2, \tag{13}$$

where \mathcal{S}_m is the z -component of the pseudospin-1 operator at the m trimer and D the trigonal splitting which depends on the SMOC. As shown in Fig. 2 the overall energy level structure of the cluster *i. e.* level splittings and degeneracies remain unaffected by anisotropies in the SMOC, $\lambda_{xy} \neq \lambda_z$ and/or intracluster exchange $J_F \neq 0$.

III. TWO COUPLED TRIANGULAR CLUSTERS

We now consider two triangular coupled clusters. We analyze the electronic structure of two nearest neighbor triangular clusters as arranged in Mo₃S₇(dmit)₃ crystals

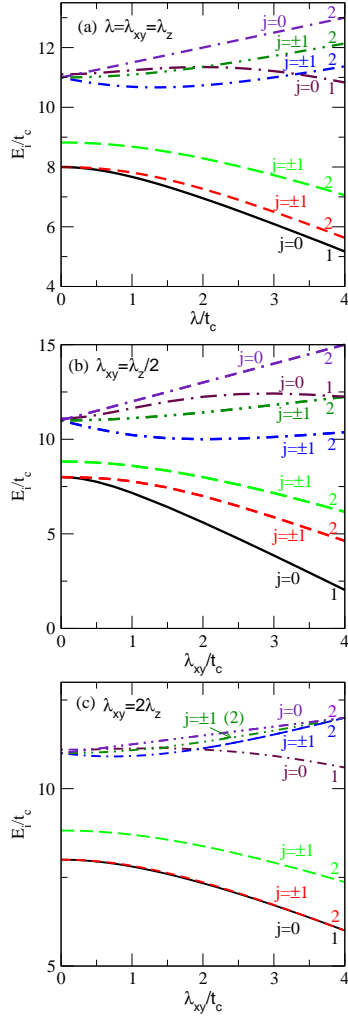


FIG. 2: Dependence of electronic structure of isolated triangular clusters with SMOC. The electronic structure of our model hamiltonian, $H = H_0 + H_{SMOC} + H_{U-J_F}$, with $N = 4$ electrons for $U = 10t_c$ and $J_F = 0$ is shown for different SMOC anisotropy ratios, λ_{xy}/λ_z . We compare (a) the isotropic SMOC case, $\lambda = \lambda_{xy} = \lambda_z$, with anisotropic ratios shown in (b) $\lambda_{xy} = \lambda_z/2$ and (c) $\lambda_{xy} = 2\lambda_z$. The eigenstates are classified according to the z -component of total angular momentum $j = k + \sigma$. The numbers denote energy level degeneracies. For $J_F \neq 0$ the electronic structure of the isolated cluster remains very similar conserving the energy level degeneracies shown.

and shown in Fig. 3. In Fig. 3(a) we show two nearest-neighbor clusters in the $a-b$ plane whereas in (b) we show two nearest-neighbor clusters along the c -direction. The molecules in the "dumbbell" configuration of Fig. 3(a) are related by inversion symmetry as in $\text{Mo}_3\text{S}_7(\text{dmit})_3$. Molecules in the "tube" configuration of Fig. 3(b) are only related by a rigid translation along the c -axis but no inversion symmetry between the molecules is present. We will first obtain exact results of the electronic structure of two coupled trimers in the two arrangements of Fig. 3 relevant to $\text{Mo}_3\text{S}_7(\text{dmit})_3$. The energy level structure

gives key information about the type of spin exchange acting between the effective pseudospins localized at each trimer. These exact results are also used to benchmark perturbation theory calculations.

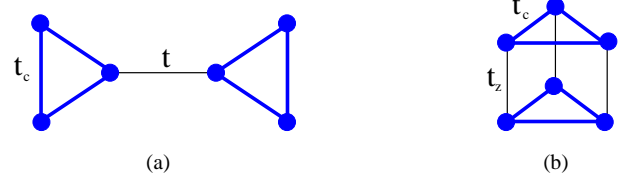


FIG. 3: The two arrangements of two neighbor trimers relevant to $\text{Mo}_3\text{S}_7(\text{dmit})_3$ crystals. In (a) we show two neighbor trimers in the $a-b$ plane whereas in (b) the two trimers are arranged along the c -direction. In the dumbbell arrangement (a) the two molecules are related by inversion symmetry through the midpoint of the bond while in the tube arrangement (b) they are related by translation symmetry. Only these symmetries are preserved in the two-coupled cluster calculations described in the text mimicking the symmetries of the $\text{Mo}_3\text{S}_7(\text{dmit})_3$ crystal.

A. Electronic structure

Consider a model of two trimers, ℓ and m coupled by H_{kin} :

$$H = H_\ell + H_m + H_{kin}, \quad (14)$$

where H_ℓ is the Hubbard-Heisenberg model of an isolated trimer, ℓ , in the presence of SMOC as introduced previously, Eq. (11) in Sec. IIB. The hopping between two neighbor clusters is described through, H_{kin} . As shown in Fig. 3, in the dumbbell arrangement, there is only one hopping amplitude connecting the trimers, so H_{kin} reads

$$H_{kin}^{dumbbell} = -t \left(a_{\ell 1\sigma}^\dagger a_{m 1\sigma} + a_{m 1\sigma}^\dagger a_{\ell 1\sigma} \right), \quad (15)$$

which connects, say, site 1 of the ℓ -cluster with site 1 of the m -cluster. Here $a_{mi\sigma}^\dagger$ annihilates (creates) an electron with spin σ in the i th Wannier orbital on molecule m . The molecular label is suppressed throughout Section II. In the tube arrangement the three vertices of the two clusters are connected by a hopping, t_z , and H_{kin} , reads

$$H_{kin}^{tube} = -t_z \sum_{i\sigma} \left(a_{\ell i\sigma}^\dagger a_{m i\sigma} + a_{m i\sigma}^\dagger a_{\ell i\sigma} \right). \quad (16)$$

We have exactly diagonalized model (14) for two coupled triangular clusters in the presence of SMOC. We consider the case in which each cluster is filled with $N = 4$ electrons which is the relevant case for $\text{Mo}_3\text{S}_7(\text{dmit})_3$ crystals. In Fig. 4(a) and (b) we show the dependence of the eigenenergies, E_i , on $\lambda = \lambda_{xy} = \lambda_z$ (isotropic SMOC) for $U = 10t_c$, $t = 0.785t_c$ and $J_F = 0$ in the dumbbell (a) and tube (b) arrangements. For $\lambda = 0$ we find that the

eigenspectrum of the coupled trimers consist of a ground state non-degenerate singlet, a triplet and a pentuplet. This is the eigenspectrum expected for an *isotropic* antiferromagnetic exchange interaction between two localized $S = 1$ moments¹⁸. As λ is increased the energy levels are split partially removing $\lambda = 0$ degeneracies. The ground state of the coupled trimers is found to be non-degenerate for any value of λ .

On the other hand, the triplet combination of the two pseudospin-1, located at each trimer, is split into a singlet and a doublet while the pentuplet is split into two doublets and a singlet. The energy levels are found to depend quadratically on λ : $E_i \propto \lambda^2$, indicating the absence of the linear DM contribution, as expected since there is an inversion symmetry center at the midpoint between the two triangular clusters^{16,21}. The level splittings found when coupling the two clusters shown in Fig. 4 correspond to the trigonal crystal field of Eq. (13) induced by λ acting on an *isotropic* antiferromagnetic Heisenberg model. Hence, the level spectra is consistent with the C_3 symmetry of the isolated triangular clusters despite the lower C_i symmetry of the dumbbell configuration of the two clusters in the presence of SMOC. This issue will be discussed further below. In Figs. 4(c) and (d) we show the dependence of E_i on t for fixed SMOC, $\lambda = 0.25t$ and $\lambda = t$. In both cases the eigenenergies depend quadratically on t , $E_i \propto t^2$ up to large values of $t/t_c \sim 1$ indicating that second order perturbation theory ($O(t^2)$) is reliable. Below, we will further analyze the accuracy of the $O(t^2)$ calculation for the model parameters that are relevant to $\text{Mo}_3\text{S}_7(\text{dmit})_3$ crystals.

When two trimers are coupled through the hopping in the dumbbell arrangement, the C_3 (trigonal) symmetry of the isolated trimers is lowered to C_i (triclinic) symmetry. This is a somewhat subtle point. In the absence of SMOC the dumbbell model is D_{2h} symmetric as it also contains three mutually perpendicular two-fold rotation axes (cf. Fig. 3). If two molecules, ℓ and m are related to one another by inversion symmetry then the pseudovectorial nature of angular momenta requires that the SMOC is equal on both molecules: $\lambda_{\ell,xy} = \lambda_{m,xy}$ and $\lambda_{\ell,z} = \lambda_{m,z}$. On the other hand if two molecules are related by a π -rotation about, say, the z -axis this yields $\lambda_{\ell,z} = \lambda_{m,z}$, but $\lambda_{\ell,xy} = -\lambda_{m,xy}$. This leads to significant changes in the effective interactions between the molecular spins, which we have discussed elsewhere.^{11,16} Thus the case $\lambda_{\ell,xy} = \lambda_{m,xy}$ and $\lambda_{\ell,z} = \lambda_{m,z}$, which we consider here, lowers the symmetry to C_i .

Since C_i has only one-dimensional irreducible representations one expects the level degeneracies associated with the trigonal symmetry to be fully lifted in the presence of SMOC. We will denote these level splittings as triclinic splittings. We have already shown that for $J_F = 0$ two coupled clusters in the dumbbell arrangement display level degeneracies consistent with trigonal symmetry. However, for $J_F \neq 0$ these level degeneracies are removed. In particular, it is interesting to monitor the difference in energy between the second and third eigen-

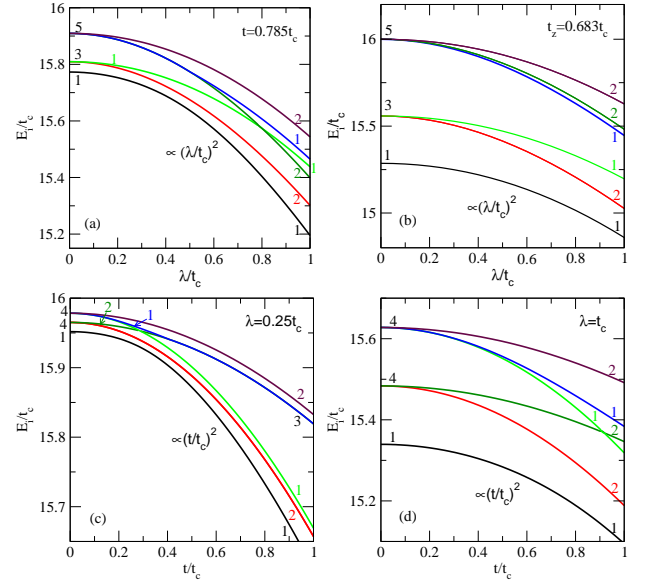


FIG. 4: Exact energy level spectra of two coupled trimers. The plots show exact eigenstates of model (14) for $U = 10t_c$ and isotropic SMOC, $\lambda = \lambda_{xy} = \lambda_z$ and $J_F = 0$. The dependence of eigenstates, E_i , with λ for $t = 0.785t_c$ are shown for the dumbbell (a) and tube arrangement (b). These plots show an $E_i \propto \lambda^2$ dependence. In (c) and (d) we fix λ and analyze the dependence of E_i on the hopping, t , in the dumbbell configuration. A quadratic dependence, $E_i \propto t^2$, is found for both weak SMOC, $\lambda = 0.25t_c$ in (a) and strong SMOC, $\lambda = t_c$ in (d). The numbers denote the energy level degeneracies.

states, $E_3 - E_2$, to quantify the departure from trigonal symmetry *i. e.* the triclinic splitting. In Fig. 5 we show the dependence of $E_3 - E_2$, on the intracluster Heisenberg exchange, J_F , for the dumbbell arrangement. For $J_F = 0$ no level splitting is present whatever the λ_{xy}/λ_z ratio is. However, a triclinic splitting arises as J_F is increased until it saturates at sufficiently large J_F . The largest splittings are found when SMOC is anisotropic, particularly when $\lambda_{xy}/\lambda_z > 1$. This is in contrast to the tube arrangement for which no triclinic splittings are found for any value of J_F and/or λ_{xy}/λ_z ratio.

The differences in the level degeneracies observed between dumbbells and tubes can be ascribed to the different symmetry of the two cluster arrangements. While tubes respect the trigonal symmetry of the isolated trimers, dumbbells break C_3 symmetry. As a consequence of this, the kinetic energy between two trimers in the tube arrangement expressed in the momentum basis is diagonal:

$$H_{kin}^{tube} = -t_z \sum_k \left(b_{\ell k \sigma}^\dagger b_{m k \sigma} + b_{m k \sigma}^\dagger b_{\ell k \sigma} \right), \quad (17)$$

where $k = 0, \pm 1$, are the allowed momenta at each trimer. This simply reflects the conservation of the molecular orbital momentum of isolated trimers. In contrast, for dumbbells, the kinetic energy contains off-diagonal hop-

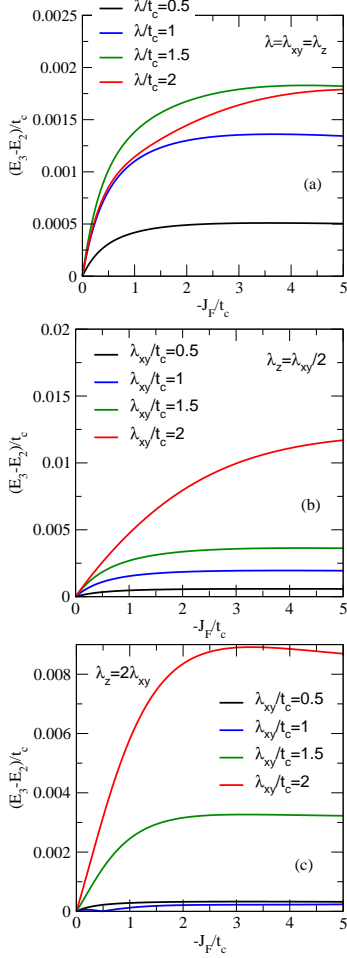


FIG. 5: Triclinic anisotropies induced by the Heisenberg intracluster exchange, J_F , and SMOC, λ_{xy} , λ_z , for different ratios and strengths of SMOC. The energy difference between the exact third and second lowest energy levels for the dumbbell configuration is shown as a function of $-J_F$ (ferromagnetic direct exchange). We have fixed $U = 10t_c$, $t = 0.785t_c$ in all figures. In (a) we show results for the Hubbard-Heisenberg model with isotropic SMOC, $\lambda = \lambda_{xy} = \lambda_z$, (b) $\lambda_z = \lambda_{xy}/2$ and in (c) $\lambda_z = 2\lambda_{xy}$. In contrast, in the case of the tube arrangement the energy splittings are zero: $E_3 - E_2 = 0$, for any finite value of J_F and λ_{xy}/λ_z ratio due to the trigonal (C_3) symmetry in that case.

ping matrix elements:

$$H_{kin}^{dumbbell} = -\frac{t}{3} \sum_{k_1 k_2} \left(b_{\ell k_1 \sigma}^\dagger b_{m k_2 \sigma} + b_{m k_2 \sigma}^\dagger b_{\ell k_1 \sigma} \right), \quad (18)$$

showing that the orbital momentum is not conserved in this case due to breaking of trigonal symmetry. Based on symmetry arguments we should then expect no triclinic splittings when two trimers are coupled in a tube. This is consistent with the numerical results shown in Fig. 5. Since the symmetry of the dumbbell arrangement corresponds to the C_i group, which has only one-dimensional irreducible representations, we should then expect non-

degenerate levels in the spectrum for non-zero SMOC. However, we find that the actual form of the Coulomb matrix affects the level degeneracies in this case and only when the intracluster exchange is non-zero, $J_F \neq 0$, are the level degeneracies completely lifted. Hence, the degeneracies observed in the dumbbell case for $J_F = 0$ should be due to an additional hidden symmetry.

The relation between the Coulomb interactions and the existence of spin exchange anisotropies has been discussed in the context of transition metal oxides with significant SOC²⁰. It has been argued that the spin exchange anisotropies depend crucially on the form of the hopping matrix between the nearest-neighbor transition metal ions and of the relevant Coulomb interactions acting between the electrons in the localized ion orbitals. In highly symmetric lattice models in which the hopping matrix is diagonal, i.e. that only orbitals of the same type at each ion are connected by hopping amplitudes, then off-diagonal Coulomb exchange between orbitals is needed to generate anisotropic exchange couplings. Magnetic anisotropies in models containing only direct Coulomb interaction independent of the orbitals involved are also possible but only in very low symmetry lattice models in which different hopping amplitudes connect the different orbitals.

As shown above, dumbbells have a lower symmetry (C_i) than tubes (C_3) leading to the different types of hopping matrices described through Eq. (17) and Eq. (18). Our analysis shows that level splittings in the dumbbells only arise when $J_F \neq 0$. Based on these previous studies we would then conclude that the dumbbell configuration is not sufficiently low-symmetric to lead to level splittings (and exchange coupling anisotropies) since the hopping matrix between two neighbor clusters is independent of the momentum at each cluster and always equal to $t/3$ as shown in Eq. (18). This is in contrast to the lower symmetry model of Ref. 20 in which the hopping amplitudes between orbitals of neighboring ions depends on the orbitals involved. On the other hand, in the absence of a magnetic field, the higher symmetry of the tube arrangement, forbids triclinic splittings even for a finite J_F .

B. Second order perturbation theory in the intercluster hopping

In order to derive a low energy effective hamiltonian for the two coupled clusters we now perform perturbation theory calculations to $O(t^2)$. The expression of the effective hamiltonian for two coupled clusters with N elec-

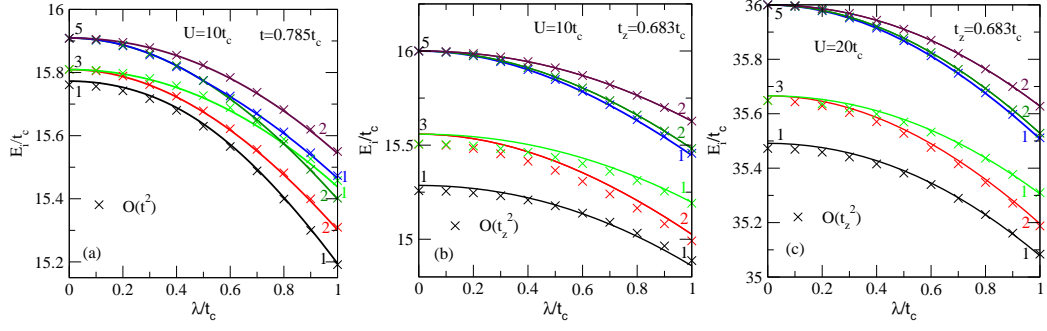


FIG. 6: Comparison between the exact energy spectrum and the eigenenergies obtained from the second order $O(t^2)$ effective hamiltonian, $H_{eff}^{(2)}$ (21). In (a) we show the comparison for the dumbbell arrangement with $U = 10t_c$ and $t = 0.785t_c$ whereas in (b) for the tube arrangement for $U = 10t_c$ and $t_z = 0.683t_c$. In (c) we show the tube arrangement for $U = 20t_c$ and $t_z = 0.683t_c$. The ratios of the hopping amplitudes t/t_c and t_z/t_c taken here are those obtained from *ab initio* calculations¹⁰ performed on $\text{Mo}_3\text{S}_7(\text{dmit})_3$.

trons in each cluster reads

$$\begin{aligned}
 H_{eff}^{(2),conf} = & E_0(N, j_{\ell z})|N, j_{\ell z}\rangle\langle N, j_{\ell z}| \\
 & + E_0(N, j_{mz})|N, j_{mz}\rangle\langle N, j_{mz}| \\
 & + \sum_{|m_0\rangle} \frac{H_{kin}^{conf}|m_0\rangle\langle m_0|H_{kin}^{conf}}{2E_0(N, 0) - \langle m_0|H_0 + H_U + H_{SMOC}|m_0\rangle},
 \end{aligned} \tag{19}$$

where $E_0(N, j_{iz})$, is the energy of the isolated trimer, i , with $j_{iz} = 0, \pm 1$ with N electrons ($N = 4$ in the case of

interest here), with corresponding eigenstate $|N, j_{iz}\rangle$. In the expression above we are implicitly assuming that the ground state of isolated uncoupled trimers is three-fold degenerate even for non-zero SMOC. From a comparison to exact results and the canonical transformation, discussed below, we find that this approximation is very accurate for the parameter regime analyzed. The $\{|m_0\rangle\}$ are the whole set of virtual excitations in which an electron is transferred from one cluster to the other and read

$$|m_0\rangle = |N-1, \gamma_\ell\rangle|N+1, \gamma_m\rangle = \sum_{\mu_\ell, \mu_m} A_{\gamma_\ell}(N-1, \mu_\ell) A_{\gamma_m}(N+1, \mu_m) |N-1, \mu_\ell\rangle |N+1, \mu_m\rangle, \tag{20}$$

where $A_{\gamma_i}(N \pm 1, \mu_i) = \langle N \pm 1, \mu_i | N \pm 1, \gamma_i \rangle$. The index γ_i denotes the excitations and μ_i runs over the Hilbert state configurations with $N \pm 1$ electrons on trimer $i =$

ℓ, m .

Introducing these states in Eq. (19) we find for a given configuration of the coupled clusters

$$\begin{aligned}
 H_{eff}^{(2),conf} = & E_0(N, j_{\ell z})|N, j_{\ell z}\rangle\langle N, j_{\ell z}| + E_0(N, j_{mz})|N, j_{mz}\rangle\langle N, j_{mz}| \\
 & + t_{conf}^2 \sum_{\gamma_\ell, \gamma_m} \sum_{\sigma, \sigma'} \sum_{\mu_\ell, \nu_m, \mu'_\ell, \nu'_m} A_{\gamma_\ell}(N-1, \mu_\ell) A_{\gamma_m}(N+1, \nu_m) A_{\gamma_\ell}^*(N-1, \mu'_\ell) A_{\gamma_m}^*(N+1, \nu'_m) \times \\
 & \frac{c_\ell^\dagger 1_\sigma c_{m1\sigma} |N-1, \mu_\ell\rangle |N+1, \nu_m\rangle \langle N+1, \nu'_m| \langle N-1, \mu'_\ell| c_{m1\sigma'}^\dagger c_{\ell1\sigma'}}{\Delta\epsilon(N-1, \gamma_\ell; N+1, \gamma_m)} \\
 & + t_{conf}^2 \sum_{\gamma_\ell, \gamma_m} \sum_{\sigma, \sigma'} \sum_{\mu_m, \nu_\ell, \mu'_m, \nu'_\ell} A_{\gamma_\ell}(N+1, \nu_\ell) A_{\gamma_m}(N-1, \mu_m) A_{\gamma_m}^*(N-1, \mu'_m) A_{\gamma_\ell}^*(N+1, \nu'_\ell) \times \\
 & \frac{c_{m1\sigma}^\dagger c_{\ell1\sigma} |N-1, \mu_m\rangle |N+1, \nu_\ell\rangle \langle N+1, \nu'_\ell| \langle N-1, \mu'_m| c_{\ell1\sigma'}^\dagger c_{m1\sigma'}}{\Delta\epsilon(N-1, \gamma_m; N+1, \gamma_\ell)},
 \end{aligned} \tag{21}$$

where $conf = \text{dumbbell}, \text{tube}$. We take $t_{dumbbell} = t$ and $t_{tube} = t_z$ and we define the excitation energies as $\Delta\epsilon(N-$

$$1, \gamma_\ell; N+1, \gamma_m) = 2E_0(N) - (E_{\gamma_\ell}(N-1) + E_{\gamma_m}(N+1)).$$

It is important to test the reliability of the present second order perturbative calculation for the values of the inter cluster hopping amplitudes relevant to $\text{Mo}_3\text{S}_7(\text{dmit})_3$ crystals. We have checked the accuracy of the second order perturbation theory calculations by comparing the nine lowest energy eigenstates with the exact eigenspectrum. From Fig. 6 we conclude that the second order, $O(t^2)$, calculation is very accurate in the dumbbell arrangement with $U = 10t_c$, even for the large hopping amplitude, $t = 0.785t_c$ relevant to $\text{Mo}_3\text{S}_7(\text{dmit})_3$ crystals. In the tube arrangement, comparable accuracies can be achieved but at higher U values as can be inferred from comparing Fig. 6(b) with Fig. 6(c). The reason for the poorer accuracy attained in the tube configuration is the presence of stronger charge fluctuations^{17,22} due to the fact that particles can be exchanged between the two clusters through $\sim t_z^2/t_c$ processes without paying energy cost U .¹⁶ In contrast, in the dumbbell case, since particles can only be exchanged through the single hopping connecting the two vertices there is always an energy cost U inherent to the exchange process $\sim 4t^2/U$. In spite of this, at sufficiently large values of U we find that the second order perturbation theory is sufficiently accurate for both the dumbbell and tube arrangements even for the large values of $t = 0.785t_c$ and $t_z = 0.683t_c$ extracted from DFT.^{10,12} We will use the second order perturbative hamiltonian, $H_{eff}^{(2)}$, as the starting point to extract a low energy effective spin model of the crystal.

IV. EFFECTIVE MAGNETIC SPIN EXCHANGE MODEL

In the previous section we derived a low energy hamiltonian, $H_{eff}^{(2)}$, which describes the effective interaction between the pseudospin-1 degrees of freedom on two neighboring clusters. We would now like to have an explicit form of this low energy hamiltonian in terms of such pseudospin operators. In order to determine the actual analytical form of the pseudospin exchange hamiltonian, we have performed a canonical transformation. Analytical

expressions of the pseudospin model valid to $O(\lambda^2)$ and $O(t^2)$, are obtained assuming a $t - J$ model for the triangular clusters. By equating the matrix elements of the effective pseudospin exchange hamiltonian obtained from the canonical transformation to the matrix elements of $H_{eff}^{(2)}$ evaluated in the low energy subspace, $\{|j_\ell, j_m\rangle\}$, with $j_\ell, j_m = 0, \pm 1$, we are able to extract the parameters entering the pseudospin exchange model.

A. Canonical transformation for a nearly degenerate low-energy subspace

Consider an arbitrary Hamiltonian, $H = H_0 + H_1$ where $H_0 = \sum_\nu P_\nu H P_\nu$, $H_1 = \sum_{\mu \neq \nu} P_\nu H P_\mu$, and P_ν is a projector onto the ν th subspace. Now define $H(\varepsilon) = H_0 + \varepsilon H_1$. Let

$$\begin{aligned} \overline{H}(\varepsilon) &\equiv e^{-i\varepsilon S} H(\varepsilon) e^{i\varepsilon S} \\ &= H_0 + \varepsilon (H_1 + i[H_0, S]) \\ &\quad + \frac{\varepsilon^2}{2} (2i[H_1, S] - [[H_0, S], S]) + \dots \end{aligned} \quad (22)$$

We choose S so that the linear term vanishes, i.e., such that $iH_1 = [H_0, S]$. This implies that

$$P_\mu H P_\nu (1 - \delta_{\mu\nu}) + i P_\mu H P_\mu (P_\mu S P_\nu) - i (P_\mu S P_\nu) P_\nu H P_\nu = 0. \quad (23)$$

because $P_\mu P_\nu = P_\mu \delta_{\mu\nu}$ and $\sum_\mu P_\mu = 1$. For $\mu = \nu$ this yields $P_\mu S P_\mu = \gamma P_\mu$ for $\gamma \in \mathbb{C}$. While, for $\mu \neq \nu$ we find

$$i P_\mu H P_\nu = P_\mu H P_\mu (P_\mu S P_\nu) - (P_\mu S P_\nu) P_\nu H P_\nu \quad (24)$$

If we choose the projectors such that they project onto *strictly* degenerate subspaces then $P_\mu H P_\mu = \langle P_\mu H P_\mu \rangle$

$$P_\mu S P_\nu = \frac{i P_\mu H P_\nu}{\langle P_\mu H P_\mu \rangle - \langle P_\nu H P_\nu \rangle} \quad (25)$$

Therefore, keeping only second order $O(\varepsilon^2)$ terms, we find that

$$\begin{aligned} \overline{H} &\equiv \overline{H}(1) = H_0 + \frac{i}{2} [H_1, S] \\ &= \sum_\mu P_\mu H P_\mu - \frac{1}{2} \sum_{\mu \neq \nu} \sum_{\mu' \neq \nu'} P_\mu H P_\nu H P_{\mu'} \left(\frac{1}{\langle P_\nu H P_\nu \rangle - \langle P_{\mu'} H P_{\mu'} \rangle} + \frac{1}{\langle P_\nu H P_\nu \rangle - \langle P_\mu H P_\mu \rangle} \right) \end{aligned} \quad (26)$$

Finally, we find the effective low-energy Hamiltonian by projecting onto the low-energy subspace, henceforth denoted \mathcal{L} . Here it is convenient to associate all of the subspaces with the states chosen so that the low energy

subspace is diagonal, i.e., $P_\mu H P_\nu = 0$ if both μ and $\nu \in \mathcal{L}$. (This is always possible provided we can solve the problem restricted purely to \mathcal{L} , as in elementary degenerate perturbation theory.) We then find that

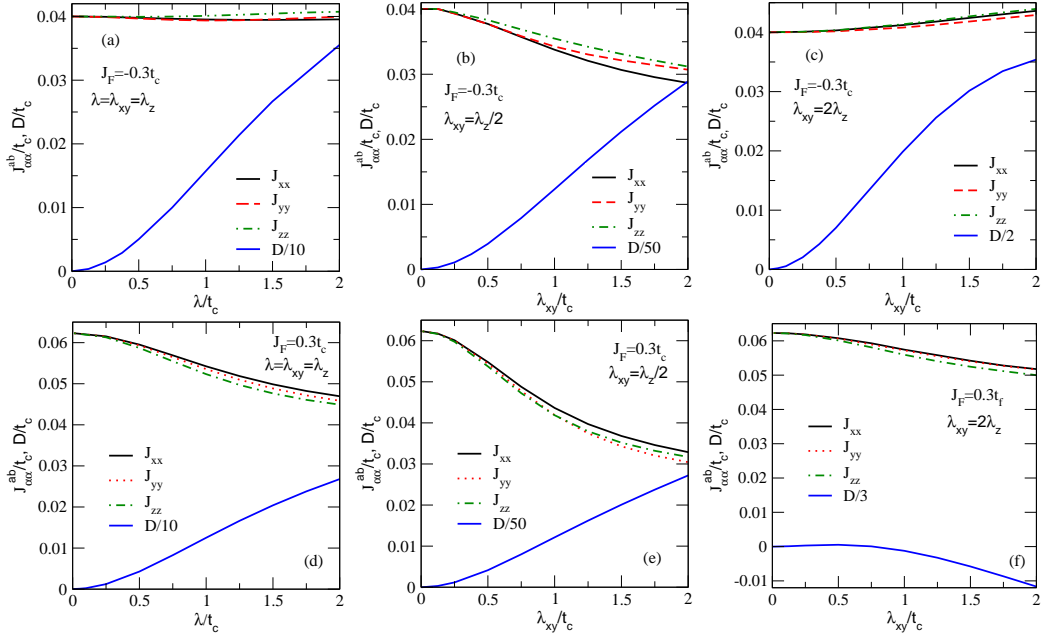


FIG. 7: Anisotropic exchange couplings and trigonal splitting in the $a - b$ plane of trinuclear complexes. The dependence on SMOC of the parameters entering the model (28) are shown for $U = 10t_c$. The hopping between the trimers is $t = 0.785t_c$. In the upper row panels we show the dependence on SMOC of the exchange couplings, $J_{\alpha\alpha}$ and the trigonal splitting, D , for different λ_{xy}/λ_z ratios in the presence of an intraccluster ferromagnetic coupling, $J_F = -0.3t_c$: (a) $\lambda_{xy}/\lambda_z = 1$, (b) $\lambda_{xy}/\lambda_z = 1/2$ and (c) $\lambda_{xy}/\lambda_z = 2$. In the lower row panels [(d), (e) and (f)] we show the same cases but for an intraccluster antiferromagnetic exchange: $J_F = 0.3t_c$.

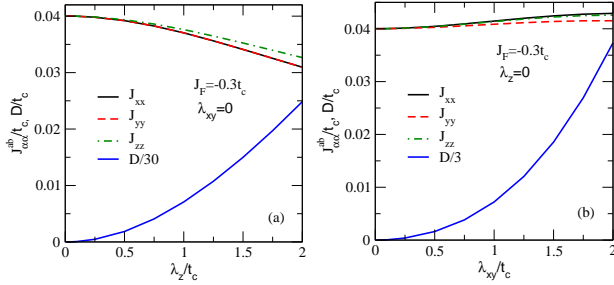


FIG. 8: Anisotropic exchange couplings in the $a - b$ plane of trinuclear complexes in the limit of extreme SMOC anisotropies. The dependence on SMOC of the parameters entering model (28) are shown for $U = 10t_c$ and $J_F = -0.3t_c$. The hopping between the trimers is $t = 0.785t_c$. We compare different ratios of the SMOC: (a) $\lambda_{xy} = 0$ and (b) $\lambda_z = 0$.

$$\begin{aligned}
 H_{\text{eff}} &\equiv P_{\mathcal{L}} \bar{H} P_{\mathcal{L}} \\
 &= \sum_{\mu \in \mathcal{L}} P_{\mu} H P_{\mu} - \frac{1}{2} \sum_{\mu, \mu' \in \mathcal{L}} \sum_{\nu \notin \mathcal{L}} \left(\frac{P_{\mu} H P_{\nu} H P_{\mu'}}{\langle P_{\nu} H P_{\nu} \rangle - \langle P_{\mu'} H P_{\mu'} \rangle} + \frac{P_{\mu} H P_{\nu} H P_{\mu'}}{\langle P_{\nu} H P_{\nu} \rangle - \langle P_{\mu} H P_{\mu} \rangle} \right), \quad (27)
 \end{aligned}$$

where $P_{\mathcal{L}} = \sum_{\mu \in \mathcal{L}} P_{\mu}$. In the case that \mathcal{L} is strictly degenerate this reduces to the standard result. In the case where there is a small continuous spread of energies in \mathcal{L} and these are treated as a single subspace, as in the derivation of the $t - J$ model, a similar result holds but

is approximate because the replacement of $P_{\mu} H P_{\mu}$ by its expectation value in Eq. (25) is no longer exact.

Based on the canonical transformation described above we derive an effective hamiltonian describing the exchange between pseudo spin-1 moments on neighboring

clusters ℓ and m described through the spin operators, \mathcal{S}_ℓ^α and \mathcal{S}_m^α , respectively. For two trimers in the ab plane, the exchange hamiltonian between a pseudospin-one moments on cluster ℓ , \mathcal{S}_ℓ and another one on cluster m , \mathcal{S}_m reads

$$H_{\text{eff}}^{ab} = \sum_{\langle \ell m \rangle_{\alpha\beta}} J_{\alpha\beta}^{ab} \mathcal{S}_\ell^\alpha \mathcal{S}_m^\alpha + \sum_\ell \left\{ D(\mathcal{S}_\ell^z)^2 + [K_{\pm\pm} \mathcal{S}_\ell^+ \mathcal{S}_\ell^+ + K_{z\pm} \mathcal{S}_\ell^z \mathcal{S}_\ell^x + H.c.] \right\}, \quad (28)$$

with $J_{\alpha\beta}^{ab} = J_{\beta\alpha}^{ab}$, $\alpha, \beta = x, y, z$ and angled brackets imply that the sum is over nearest neighbors only, avoiding double counting. On the other hand, the effective hamiltonian describing two nearest-neighbor trimers in the c -direction reads

$$H_{\text{eff}}^c = D \sum_\ell (\mathcal{S}_\ell^z)^2 + \sum_{\langle lm \rangle_{\alpha\beta}} J_{\alpha\beta}^c \mathcal{S}_\ell^\alpha \mathcal{S}_m^\beta + \sum_{\langle lm \rangle_{\alpha\beta}} P_{\alpha\beta} \mathcal{S}_\ell^\alpha \mathcal{S}_\ell^\beta \mathcal{S}_m^\alpha \mathcal{S}_m^\beta, \quad (29)$$

where the anisotropic biquadratic couplings, $P_{\alpha\beta} = P_{\beta\alpha}$, obey $P_{zz} = 2P_{zx} = 2P_{zy}$ and $P_{xx} = P_{yy} = P_{xy} = 0$.

Finally, the full effective spin exchange model between the pseudo spin-1 in the lattice reads

$$H_{\text{eff}} = H_{\text{eff}}^{ab} + H_{\text{eff}}^c. \quad (30)$$

This expression neglects ‘three molecule’ terms analogous to the ‘three site’ terms neglected in the usual formulation of the t - J model.^{23,24}

The above two models (28) and (29) are our starting point. As stated above, the parameters governing the spin exchange between molecules ℓ and m in our spin exchange hamiltonian, H_{eff} , are obtained through the equations

$$\begin{aligned} \langle j_\ell, j_m | H_{\text{eff}}^{ab} | j_\ell, j_m \rangle &= \langle j_\ell, j_m | H_{\text{eff}}^{(2), \text{dumbbell}} | j_\ell, j_m \rangle, \\ \langle j_\ell, j_m | H_{\text{eff}}^c | j_\ell, j_m \rangle &= \langle j_\ell, j_m | H_{\text{eff}}^{(2), \text{tube}} | j_\ell, j_m \rangle, \end{aligned} \quad (31)$$

where $H_{\text{eff}}^{(2), \text{conf}}$ is our second order effective hamiltonian given in Eq. (21) for either the dumbbell or the tube configurations. The above equations are solved for a given set of parameters: U , J_F , t_c , t , t_z , λ_{xy} , and λ_z entering our original microscopic model (1).

B. Anisotropic exchange in the ab -plane

We have explored anisotropies arising in the exchange couplings of our effective pseudospin model, Eq. (30). We find that the exchange coupling tensor for two clusters related by inversion symmetry (as in the $a-b$ planes of $\text{Mo}_3\text{S}_7(\text{dmit})_3$) is diagonal: $J_{\alpha\beta}^{ab} = J_{\alpha\alpha}^{ab} \delta_{\alpha\beta}$. The non-pseudospin-conserving $K_{\alpha\beta}$ terms are zero for $J_F = 0$

and non-zero but very small ($\sim 10^{-4}t_c$) for the parameter regimes explored so they will not be considered further here.

For $J_F = 0$, the diagonal couplings are almost isotropic, $J_{xx}^{ab} = J_{yy}^{ab} = J_{zz}^{ab}$ as shown previously (see Fig. 4(a) of Ref. [11]) consistent with the lack of triclinic splittings observed in the exact calculation of the energy spectrum for the two clusters in the dumbbell configuration displayed in Fig. 5. As shown in Fig. 7 anisotropic exchange couplings $J_{xx} \neq J_{yy} \neq J_{zz}$ arise when $J_F \neq 0$, which are consistent with the triclinic splittings found in the exact level spectrum of Fig. 5.

Comparing the results shown in Fig. 7 for different λ_{xy}/λ_z ratios, we observe how the anisotropies in the exchange couplings are enhanced for $\lambda_{xy}/\lambda_z \neq 1$. In fact, larger anisotropies are found occur for $\lambda_{xy} = \lambda_z/2$, which is the parameter regime relevant to $\text{Mo}_3\text{S}_7(\text{dmit})_3$ crystals.¹⁰ Also note from Fig. 7 the strong dependence of the magnitude of D with the SMOC anisotropy. As shown in Fig. 7, the trigonal splitting, D , increases rapidly with SMOC, becoming equal to the exchange couplings, $D \sim J_{\alpha\alpha}^{ab}$ at $\lambda \approx 0.45t_c$ ($\lambda = \lambda_{xy} = \lambda_z$), at $\lambda_{xy} \approx 0.22t_c$ ($\lambda_{xy} = \lambda_z/2$) and at $\lambda_{xy} \approx 1.045t_c$ ($\lambda_{xy} = 2\lambda_z$). At sufficiently large D , $D \gg J_{\alpha\alpha}^{ab}$ we expect the D -phase, *i. e.* a tensor product of $j = 0$ states located at each cluster of the crystal. Hence, a D -phase is favored by anisotropic SMOC with $\lambda_{xy} < \lambda_z$.

In Fig. 7 we also show results for an antiferromagnetic exchange coupling inside the cluster, $J_F > 0$. This could arise in $\text{Mo}_3\text{S}_7(\text{dmit})_3$ due to superexchange via the sulphur atoms in the core or the dmit ligands. Apart from the similar spin exchange anisotropies found for $J_F = 0.3t_c$, it is worth mentioning that, in contrast to the ferromagnetic case for $\lambda_{xy} = 2\lambda_z$, we find that D becomes negative for sufficiently large SMOC. This signifies a switch of the ground state of the isolated cluster from the $j = 0$ singlet to the $j = \pm 1$ doublet. In contrast, in the ferromagnetic cases, $J_F < 0$, we have explored a large parameter set and we always find $D > 0$.

In order to understand the effect of exchange couplings with SMOC anisotropy, we show in Fig. 8 exchange couplings, $J_{\alpha\alpha}^{ab}$, and D in two extreme cases: $\lambda_{xy} = 0$ and $\lambda_z = 0$ with $J_F = -0.3t_c$. The $J_{\alpha\alpha}^{ab}$ are suppressed (enhanced) with SMOC for $\lambda_{xy} = 0$ ($\lambda_z = 0$). This behavior is consistent with the results shown in Fig. 7. Only when λ_{xy} is turned on, does one find that the transverse couplings become different *i. e.* $J_{xx} \neq J_{yy}$. It is worth noting the large enhancement of the trigonal splitting encountered for $\lambda_{xy} = 0$.

The effect of SMOC anisotropy on the exchange couplings found in our numerical results can be understood from previous analytical expressions (see Eqs. A1 b-d, of Ref [11]). Also the trigonal splitting is much more (more than an order of magnitude) strongly enhanced by λ_{xy} than by λ_z which is also consistent with the analytical expressions (see Eq. A1j of Ref [11]). Note that while our numerical calculations include the SMOC to all orders in perturbation theory, the analytical expressions

are limited to terms $O(\lambda^2)$.

C. Anisotropies in the exchange interactions along the c -direction

The exchange couplings between two neighboring clusters in the c -direction are shown in Fig. 9. We find a diagonal exchange tensor: $J_{\alpha\beta}^c = J_{\alpha\alpha}^c \delta_{\alpha\beta}$, with $J_{xx}^c = J_{yy}^c \neq J_{zz}^c$ for any J_F and λ_{xy}/λ_z ratio. This is in contrast to the interaction between two neighbor molecules in the ab plane discussed above in which, $J_{xx}^{ab} \neq J_{yy}^{ab} \neq J_{zz}^{ab}$, for $J_F \neq 0$ and non-zero SMOC. This is due to the fact that molecules in the tube arrangement respect the C_3 rotational symmetry of the isolated molecules around the z -axis unlike neighboring molecules in the dumbbell arrangement which allows for $J_{xx}^{ab} \neq J_{yy}^{ab}$.

The largest anisotropies with $J_{xx}^c = J_{yy}^c > J_{zz}^c$ arise in the case of anisotropic SMOC with $\lambda_{xy} = \lambda_z/2$ as shown in Fig. 9(b). The only non-negligible biquadratic exchange terms, $P_{zz} > P_{zx}$, increase rapidly with λ_{xy} starting to saturate around $\lambda \sim (1 - 1.5)t_c$. The trigonal splitting equals the exchange coupling, $D = J_{\alpha\alpha}^c$, at $\lambda_{xy} = 0.65t_c$ in the case $\lambda_{xy}/\lambda_z = 1/2$, at $\lambda_{xy} = 1.457t_c$ for $\lambda_{xy}/\lambda_z = 1$, while for $\lambda_{xy}/\lambda_z = 2$ there is no critical λ_{xy} at which $D \sim J_{\alpha\alpha}^c$. Hence, anisotropic SMOC with $\lambda_{xy} < \lambda_z$ again favors the D -phase as in the dumbbell arrangement.

Finally, we compare in Fig. 10 the dependence of the exchange couplings on J_F for $\lambda_{xy} = \lambda_z = 1$. The couplings in the ab plane, $J_{\alpha\alpha}^{ab}$ are suppressed and become gradually anisotropic, $J_{xx}^{ab} \neq J_{yy}^{ab} \neq J_{zz}^{ab}$ under the effect of J_F . This is in contrast to the exchange couplings in the c -direction which do not display larger anisotropies but rather $J_{xx}^c = J_{yy}^c \neq J_{zz}^c$ for any J_F .

V. DISCUSSION OF PROPERTIES OF THE QUASI-ONE-DIMENSIONAL PSEUDOSPIN-1 MODEL

Our analysis shows that the magnetic properties of $\text{Mo}_3\text{S}_7(\text{dmit})_3$ at strong coupling, $U \gg t_c, t, t_z, \lambda_{xy}, \lambda_z$, are captured by the model (28)-(30) with the exchange couplings obtained from our combined approach described above. On comparing $J_{\alpha\alpha}^{ab}$ in Fig. 7 with $J_{\alpha\alpha}^c$ in Fig. 9 we find that $J_{\alpha\alpha}^c \sim 5J_{\alpha\alpha}^{ab}$ for $U = 10t_c$. This is related to the fact that two clusters in the tube arrangement are connected by three hoppings so that they can exchange electrons without paying an energy cost^{11,16} $\sim U$. In contrast, neighboring clusters in the dumbbell arrangement pay energy, U , since they can only exchange particles through a single hopping connecting them. Hence, the $J_{\alpha\alpha}^{ab}$ are strongly suppressed by U in contrast to the $J_{\alpha\alpha}^c$, leading to an increase of the $J_{\alpha\alpha}^c/J_{\alpha\alpha}^{ab}$ ratio. Hence, at large U the system becomes quasi-one-dimensional consisting on a set of weakly coupled pseudo spin-1 antiferromagnetic chains.

An isotropic version of model, (29) i.e., $J_{\alpha\beta}^c = J^c \delta_{\alpha\beta}$ $P_{\alpha\beta} = P \delta_{\alpha\beta}$ and $D = 0$ is just the bilinear-biquadratic model: $H = J^c \mathbf{S}_\ell \cdot \mathbf{S}_m + P(\mathbf{S}_\ell \cdot \mathbf{S}_m)^2$, which becomes the Affleck-Kennedy-Lieb-Tasaki (AKLT) model for $P/J_c = 1/3$, which has the valence bond solid ground state and is in the Haldane phase²⁵.

We finally note that the next-nearest-neighbor exchange couplings between clusters in the c -direction can be neglected since recent estimates¹¹ suggest that they are about 20 times smaller than the nearest neighbor exchange coupling.

A. One-dimensional antiferromagnetic $S = 1$ Heisenberg chains

When no interchain coupling is present, $J^{ab} = 0$, and $D < J^c$, the system consists on a set of uncoupled one-dimensional $S = 1$ antiferromagnetic chains that are in the Haldane phase. The Haldane phase is characterized by exponentially decaying spin correlations associated with²⁶ the Haldane spin gap $\Delta_s = 0.4107(3)J^c$ to the lowest triplet state and string order. It is a symmetry-protected topological phase with nonlocal string order and fractionalized edge states²⁷⁻²⁹. Topological protection can arise from either (i) the dihedral group of π -rotations around the x and y axis, (ii) time-reversal symmetry or (iii) reflection through a plane perpendicular to the chain (or bond-center inversion symmetry, which is equivalent in one-dimension).³⁰ In the underlying fermionic model, charge fluctuations imply that topological protection can only from reflection symmetry with respect to a plane perpendicular to the c -axis at the midpoint of a bond²².

On the other hand, when $D \gg J_{\alpha\alpha}^c$, the ground state is adiabatically connected to a trivial state consisting on the tensor product of the $S_i^z = 0$ at each cluster. The lowest energy excitations of the large- D phase which reside in the $S_i^z = \pm 1$ sector, are gapped and consist of pairs of excitons and antiexcitons which can be bound. Numerical studies³¹⁻³⁴ have established that the QCP separating the large- D and Haldane phases occurs at $D/J^c \sim 0.96 - 0.971$. It has been found that in a pure spin model as the one discussed here, a quantum phase transition between the Haldane phase and the topologically trivial large- D phase is signalled by the change in sign of an inversion-symmetry-based order parameter³³ which is a non-local topological order parameter. Hence, a transition from a Haldane phase to a large- D phase occurs increasing SMOC until $D \sim J^c$.

From our analysis in Fig. 9 (b), which is the relevant SMOC ratio in $\text{Mo}_3\text{S}_7(\text{dmit})_3$, we predict a transition from the Haldane to the D -phase at $\lambda_{xy} \sim 0.65t_c$. *Ab initio* estimates of SMOC¹⁰ in $\text{Mo}_3\text{S}_7(\text{dmit})_3$ find that $\lambda_{xy} = \lambda_z/2 = 0.042t_c$, which means that the trigonal splitting is too small, $D \ll J_{\alpha\alpha}^c$, to induce a D -phase in the crystal. Moderate changes in $U = 8 - 11$ and/or $J_F = -(0.2 - 0.4)t_c$ do not change this conclusion im-

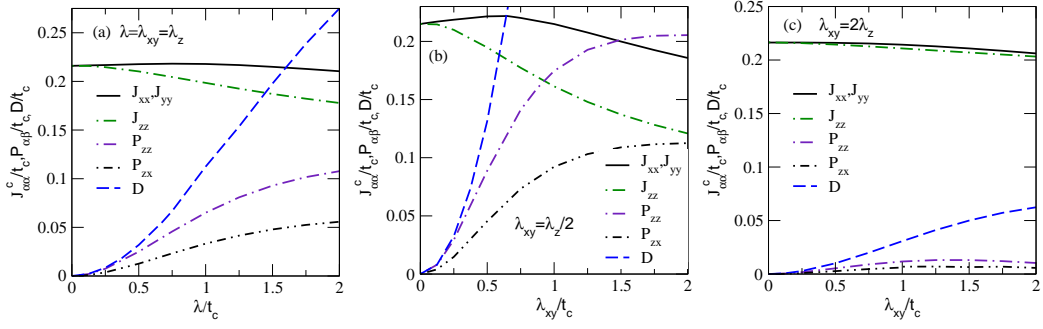


FIG. 9: Anisotropic exchange couplings in the c -direction of trinuclear complexes. The dependence on SMOC of the parameters entering the model (28) are shown for $U = 10t_c$ and $J_F = -0.3t_c$. The hopping between the trimers is $t_z = 0.683t_c$. We compare different types of SMOC: (a) $\lambda_{xy}/\lambda_z = 1$, (b) $\lambda_{xy}/\lambda_z = 1/2$ and (c) $\lambda_{xy}/\lambda_z = 2$. Note the large enhancement of the trigonal splitting, D , for anisotropic SMOC becoming the largest for $\lambda_{xy} \leq \lambda_z$. For $\lambda_{xy} = \lambda_z/2$, relevant to $\text{Mo}_3\text{S}_7(\text{dmit})_3$ crystals,¹⁰ we have that $D \sim J_{zz}^c$ at about $\lambda_{xy} = 0.65t_c$.

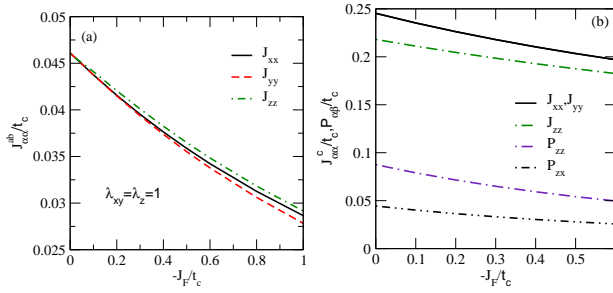


FIG. 10: Effect of the intracluster exchange, J_F , on the exchange couplings between trimers. In (a) we show the dependence of the exchange couplings in the ab -plane, J^{ab} , on $-J_F$ while in (b) we show the dependence of exchange couplings in the c -direction, J^c , on $-J_F$. We have used $U = 10t_c$, $t = 0.785$, $t_z = 0.683$ and $\lambda_{xy} = \lambda_z = 1$.

plying that the $\text{Mo}_3\text{S}_7(\text{dmit})_3$ crystal is most likely in the Haldane phase. However, in the underlying fermionic model (neglecting SMOC) the Haldane gap is suppressed by charge fluctuations.²² It is therefore interesting to speculate that charge fluctuations may also lower the critical value of D/J^c . Our results above demonstrate that the ratio D/J^c could be enhanced by moving to suitable materials containing heavier elements.⁹

B. Effect of the interchain couplings

When the quantum pseudospin-1 chains are coupled through a sufficiently strong interchain coupling, J^{ab} , the Haldane phase becomes unstable to 3D magnetic order. In previous numerical studies of weakly coupled $S = 1$ antiferromagnetic Heisenberg chains (with $D = 0$), it was estimated³⁵ that the critical value for the transition from the Haldane to the ordered 3D magnet occurs around $J^{ab}/J^c \geq (0.08 - 0.11)z \sim 0.3$, where $z = 3$ for the honeycomb lattice coordination number. Since we find that $J^{ab}/J^c \lesssim 0.2$, we expect that the ground state of

our model is in the Haldane phase when $\Delta = 0$. This critical ratio, J^{ab}/J^c , for the onset of 3D magnetic order is suppressed following the suppression of the Haldane gap by D as shown³⁶ by mean-field treatments of the interchain coupling, J^{ab} .

C. Effect of an external magnetic field

An external magnetic field suppresses the 1D quantum fluctuations and the Haldane gap, Δ_s , closes³⁷ at $h_c \sim \Delta_s$, at which a transition to a 3D ordered magnet occurs. A quantum critical region with a V-shape emerges around h_c in the temperature versus magnetic field, T - h , phase diagram^{36,38,39}. The temperature, $T \sim J^{ab}$, sets the energy scale at which 3D quantum criticality for $T < J^{ab}$ crosses over to 1D behavior for $T > J^{ab}$. Similarly the three-dimensional magnetically ordered phase found for $h > h_c$ and $T = 0$ crosses over to a gapless Tomonaga Luttinger Liquid (TLL) at temperatures $T > J^{ab}$. We note that, strictly speaking, the TLL behavior should only occur⁴⁰ in the range $J^{ab} < T < J^c$, since at too large temperatures, $T \gg J^c$, classical behavior sets in. In the presence of a nonzero and small D , with $D \ll J^c$, the lowest triplet state is split into a $j = \pm 1$ doublet with energy Δ_{\pm} above the ground state and a $j = 0$ singlet at energy Δ_0 with $\Delta_{\pm} < \Delta_0$. Hence, under an applied magnetic field, Δ_{\pm} is suppressed and the transition from the Haldane phase to the 3D ordered phase occurs around $h_c = \Delta_{\pm} < \Delta_s$. Apart from the downward shift of h_c , we can expect, qualitatively, a similar T - h phase diagram as in the case with no trigonal splitting, $D = 0$.

VI. CONCLUSIONS

Motivated by the intensive search for materials in which the Kitaev model may be realised⁴¹, we have analyzed the magnetic properties of the multinuclear

organometallic materials, such as $\text{Mo}_3\text{S}_7(\text{dmit})_3$. This material is a potential candidate for sustaining compass interactions in its hexagonal layers. In order to explore such possibilities we have derived an effective magnetic model describing the magnetic interactions between the pseudospin-1 at each molecular cluster arising from strong Coulomb repulsion, lattice structure and SMOC. In spite of the crystals being nearly isotropic, we find that the exchange coupling between nearest-neighbor pseudospins along the c -direction is much larger than between pseudospins within the hexagonal $a - b$ planes. Hence, the spin exchange model for these crystals is effectively quasi-one-dimensional. Magnetic anisotropies are found to arise under the simultaneous effect of spin orbit coupling and intra-cluster exchange interaction. These anisotropies are further enhanced by SMOC anisotropy, particularly when $\lambda_{xy} < \lambda_z$, which is naturally present in $\text{Mo}_3\text{S}_7(\text{dmit})_3$. Our analysis suggests that $\text{Mo}_3\text{S}_7(\text{dmit})_3$ may be in a Haldane phase since the model consists of weakly coupled $S = 1$ antiferromagnetic chains.

The Haldane phase is strongly sensitive to an external magnetic field. Under applied magnetic fields larger than the Haldane gap, $h > h_c \sim \Delta_s$, the Haldane phase is destroyed and a three-dimensional magnet may be stabilized. We have estimated this critical field, h_c , based on our present analysis using appropriate DFT¹⁰ parameters for $\text{Mo}_3\text{S}_7(\text{dmit})_3$ $\lambda_{xy} = \lambda_z/2 = 0.042t_c$, $t = 0.785t_c$, $t_z = 0.683t_c$, $t_c = 0.059$ eV with an onsite $U = 10t_c$ and $J_F = -0.3t_c$. Using these parameters we extract $J^c = 0.0126$ eV from our Fig. 9(b) which leads to a critical magnetic field $h_c \sim \Delta_s \sim 41.4$ T. A V-shaped quantum critical region in the $T - h$ phase diagram separating the Haldane phase from the three-dimensional magnetically ordered phase should then emerge as observed in inorganic Haldane chain materials.³⁹

Exfoliation or growth of a monolayer of $\text{Mo}_3\text{S}_7(\text{dmit})_3$, would lead to the realization of a decorated hexagonal lattice which is known to contain rich physics. We have found that at large U and no SMOC, the magnetic interactions between the pseudospin-1 would be that of a conventional nearest-neighbor antiferromagnetic Heisenberg model on an hexagonal lattice. The ground state of this model is a pure Néel antiferromagnet. However, if next-nearest neighbor antiferromagnetic couplings and/or the exchange anisotropies found here are also considered, disordered spin liquid phases⁴² may be achieved. If the relative orientation between the molecules in the crystal is modified so that inversion symmetry within the planes is broken, a DM interaction arises¹⁶ which competes with the magnetic order⁴³ which can lead to interesting spin liquid phases⁴⁴. All this illustrates how isolated layers of trinuclear organometallic complexes are ideal playgrounds to explore the quantum many-body phases realized in a decorated honeycomb lattice.

Acknowledgements.

J.M. acknowledges financial support from MINECO (MAT2015-66128-R). Work at the University of Queensland was supported by the Australian Research Council (FT13010016 and DP160100060).

APPENDIX: ELECTRONIC STRUCTURE OF ISOLATED TRIANGULAR CLUSTERS

Here, we provide the details of the electronic structure of isolated clusters with different numbers of electrons.

A. Isolated triangular cluster with five electrons

We start studying isolated trimers with $N = 1$ electrons. This is due to its intrinsic importance and due to the fact that the electronic structure of trimers with $N = 5$ electrons and $t_c, \lambda_{xy}, \lambda_z > 0$, relevant to $\text{Mo}_3\text{S}_7(\text{dmit})_3$ can be obtained from the $N = 1$ case by a particle-hole transformation switching the sign of the parameters: $t_c \rightarrow -t_c, \lambda_{xy} \rightarrow -\lambda_{xy}, \lambda_z \rightarrow -\lambda_z$ apart from a rigid energy shift.

For only one electron in the cluster, $N = 1$, the hamiltonian is just $H = H_0 + H_{SMOC}$. Since $[H, J_z] = 0$, where $J_z = L_z + S_z$, then the projection of the total momentum along the z -axis is a good quantum number. In the following we denote the basis states for a fixed number of particles, N , as $|N; j, n\rangle$ where $j = k + \sigma$ and n numbers the different possible configurations for each j -sector. Hence, in this case the possible basis states are

$$\begin{aligned} |1; 1/2, 1\rangle &= b_{0\uparrow}^\dagger |0\rangle \\ |1; 1/2, 2\rangle &= b_{1\downarrow}^\dagger |0\rangle \\ |1; -1/2, 1\rangle &= b_{0\downarrow}^\dagger |0\rangle \\ |1; -1/2, 2\rangle &= b_{-1\uparrow}^\dagger |0\rangle \\ |1; 3/2, 1\rangle &= b_{1\uparrow}^\dagger |0\rangle \\ |1; -3/2, 1\rangle &= b_{-1\downarrow}^\dagger |0\rangle. \end{aligned} \quad (32)$$

The eigenenergies, $E_n(N; j)$ of the hamiltonian are

$$\begin{aligned} E_2(1; j = \pm 3/2) &= t_c + \frac{\lambda_z}{2}, \\ E_1(1; j = \pm 1/2) &= -\frac{\lambda_z}{4} - \frac{t_c}{2} + \sqrt{\left(\frac{\lambda_z - 6t_c}{4}\right)^2 + \frac{\lambda_{xy}^2}{2}}, \\ E_0(1; j = \pm 1/2) &= -\frac{\lambda_z}{4} - \frac{t_c}{2} - \sqrt{\left(\frac{\lambda_z - 6t_c}{4}\right)^2 + \frac{\lambda_{xy}^2}{2}}. \end{aligned} \quad (33)$$

Hence the level spectra for $N = 1$ consists of three doublets with the energies given above. The ground state of the system with one electron, $N = 1$, is a doublet with

energy, E_0 . Time-reversal invariance of the hamiltonian, $[T, H] = 0$, and Kramers theorem ensures that all states should have a minimum degeneracy of two since the cluster has an odd number of electrons. Note that the level spectra of the triangular cluster with $N = 5$ electrons (one hole) would be the same as (33) but with the signs reversed: $t_c \rightarrow -t_c$, $\lambda_{xy} \rightarrow -\lambda_{xy}$, $\lambda_z \rightarrow -\lambda_z$ and with an upward rigid shift of all energies by $+2U$.

To make contact with previous work on transition metal oxides it is illustrative to consider our model hamiltonian: $H = H_0 + H_{SMOC} + H_{U-J_F}$, with H_0 , H_{SMOC} and H_{U-J_F} expressed in the (k, σ) basis as given by Eq. (9), (10) and (12), respectively. For $U, J_F = 0$, this model is reminiscent of a model previously considered⁴⁻⁶ for Ir^{4+} ions in $A_2\text{IrO}_3$ ($A=\text{Na, Li}$) compounds. In these systems, five electrons occupy the lowest t_{2g} manifold of the Ir ions which is well separated from the high energy e_g doublet. The low energy effective model for the hole in the t_{2g} manifold of the *isolated* Ir-ions includes a trigonal crystal field resulting from the surrounding oxygen octahedra and a large SOC contribution⁶: $H = \Delta(L^z)^2 + \lambda \mathbf{L} \cdot \mathbf{S}$, with $\Delta > 0$. Note that in contrast to the molecular case, the SOC is isotropic, $\lambda = \lambda_{xy} = \lambda_z$, in the case of ions/atoms.

Through the particle-hole transformation discussed above, the three-fold degenerate t_{2g} manifold of the isolated Ir ion with one hole is equivalent to our model of the isolated molecule with one electron, $N = 1$, with the signs of $\lambda = \lambda_{xy} = \lambda_z$ and t_c reversed. Full rotational symmetry is only recovered for $t_c \rightarrow 0$ in our model when $U, J_F = 0$. In that case, $[H_0 + H_{SMOC}, L] = 0$, so that the total angular momentum, L , is a good quantum number, as it should. In this situation, we find that isotropic SOC ($\lambda_{xy} = \lambda_z = \lambda$) splits the $(2L+1)(2S+1) = 6$ manifold ($L = 1, S = 1/2$) into a $j = 1/2$ doublet with energy $E_0(1; j = 1/2) = -\lambda$ and a $j = 3/2$ quadruplet with energy $E_1(1; j = 3/2) = \frac{\lambda}{2}$. This situation corresponds to removing the crystal field acting on the d -orbital manifold in transition metal oxides.

B. Isolated triangular clusters with four electrons

The basis states with $N = N_\uparrow + N_\downarrow = 4$ electrons includes states with total spin $S_z = 0$, ($N_\uparrow = 2, N_\downarrow = 2$), $S_z = 1$ ($N_\uparrow = 3, N_\downarrow = 1$) and $S_z = -1$ ($N_\uparrow = 1, N_\downarrow = 3$). Noting that basis states with total momentum k' are equivalent to k if they satisfy $k = k' \pm 3n$, we find that the basis states can be classified according to three possible values: $j = 0, \pm 1$. Since the hamiltonian does not mix states with different j , the original 15×15 matrix can be expressed in block diagonal form consisting of 5×5 matrices corresponding to $j = 0, \pm 1$. We now explicitly show the classification of the (k, σ) basis states according to $j = 0, \pm 1$ and the analytical diagonalization of the matrices corresponding to each of the j -sectors. We keep the $|N; j, n\rangle$ classification of the basis states.

1. $j = 0$ sector

The three possible configurations with $k = \sigma = 0$ are

$$\begin{aligned} |4; 0, 1\rangle &= b_{0\uparrow}^\dagger b_{-1\uparrow}^\dagger b_{0\downarrow}^\dagger b_{1\downarrow}^\dagger |0\rangle \\ |4; 0, 2\rangle &= b_{0\uparrow}^\dagger b_{1\uparrow}^\dagger b_{0\downarrow}^\dagger b_{-1\downarrow}^\dagger |0\rangle \\ |4; 0, 3\rangle &= b_{-1\uparrow}^\dagger b_{1\uparrow}^\dagger b_{-1\downarrow}^\dagger b_{1\downarrow}^\dagger |0\rangle \end{aligned} \quad (34)$$

There is only one configuration for either $k = -1, \sigma = 1$,

$$|4; 0, 4\rangle = b_{0\uparrow}^\dagger b_{-1\uparrow}^\dagger b_{1\uparrow}^\dagger b_{-1\downarrow}^\dagger |0\rangle, \quad (35)$$

or $k = 1, \sigma = -1$

$$|4; 0, 5\rangle = b_{1\uparrow}^\dagger b_{0\downarrow}^\dagger b_{-1\downarrow}^\dagger b_{1\downarrow}^\dagger |0\rangle. \quad (36)$$

Hence, the $j = 0$ Hamiltonian reduces to a 5×5 matrix:

$$H(4; j = 0) = \begin{bmatrix} -2t_c + \frac{4U}{3} - \frac{7J_F}{6} - \lambda_z & \frac{U-J_F/2}{3} & -\frac{U+J_F}{3} & 0 & 0 \\ \frac{U-J_F/2}{3} & -2t_c + \frac{4U}{3} - \frac{7J_F}{6} + \lambda_z & -\frac{U+J_F}{3} & -\frac{\lambda_{xy}}{\sqrt{2}} & \frac{\lambda_{xy}}{\sqrt{2}} \\ -\frac{U+J_F}{3} & -\frac{U+J_F}{3} & 4t_c + \frac{4U}{3} - \frac{5J_F}{3} & \frac{\lambda_{xy}}{\sqrt{2}} & -\frac{\lambda_{xy}}{\sqrt{2}} \\ 0 & -\frac{\lambda_{xy}}{\sqrt{2}} & \frac{\lambda_{xy}}{\sqrt{2}} & U + t_c - J_F + \frac{\lambda_z}{2} & 0 \\ 0 & \frac{\lambda_{xy}}{\sqrt{2}} & -\frac{\lambda_{xy}}{\sqrt{2}} & 0 & U + t_c - J_F + \frac{\lambda_z}{2} \end{bmatrix}$$

2. $j = -1$ sector

We work in the basis

$$\begin{aligned}
|4; -1, 1\rangle &= b_{0\uparrow}^\dagger b_{-1\uparrow}^\dagger b_{-1\downarrow}^\dagger b_{1\downarrow}^\dagger |0\rangle \\
|4; -1, 2\rangle &= b_{-1\uparrow}^\dagger b_{1\uparrow}^\dagger b_{0\downarrow}^\dagger b_{-1\downarrow}^\dagger |0\rangle \\
|4; -1, 3\rangle &= b_{0\uparrow}^\dagger b_{1\uparrow}^\dagger b_{0\downarrow}^\dagger b_{1\downarrow}^\dagger |0\rangle, \\
|4; -1, 4\rangle &= b_{0\uparrow}^\dagger b_{0\downarrow}^\dagger b_{-1\downarrow}^\dagger b_{1\downarrow}^\dagger |0\rangle, \\
|4; -1, 5\rangle &= b_{0\uparrow}^\dagger b_{-1\uparrow}^\dagger b_{1\uparrow}^\dagger b_{1\downarrow}^\dagger |0\rangle.
\end{aligned} \tag{37}$$

The first three states have $k = -1 = 2$, $\sigma = 0$, the fourth has $k = 0$, $\sigma = -1$ and the fifth has $k = 1 = -2$, $\sigma = 1$. The $j = -1$ hamiltonian is

$$H(4; j = -1) = \begin{bmatrix} t_c + \frac{4U}{3} - \frac{7J_F}{6} - \frac{\lambda_z}{2} & \frac{U-J_F/2}{3} & \frac{U+J_F}{3} & -\frac{\lambda_{xy}}{\sqrt{2}} & 0 \\ \frac{U-J_F/2}{3} & t_c + \frac{4U}{3} - \frac{7J_F}{6} + \frac{\lambda_z}{2} & \frac{U+J_F}{3} & 0 & 0 \\ \frac{U+J_F}{3} & \frac{U+J_F}{3} & -2t_c + \frac{4U}{3} - \frac{5J_F}{3} & 0 & -\frac{\lambda_{xy}}{\sqrt{2}} \\ -\frac{\lambda_{xy}}{\sqrt{2}} & 0 & 0 & -2t_c + U - J_F & 0 \\ 0 & 0 & -\frac{\lambda_{xy}}{\sqrt{2}} & 0 & U + t_c - J_F - \frac{\lambda_z}{2} \end{bmatrix} \tag{38}$$

3. $j = +1$ sector

It is convenient to take the basis states as the time-reversed analogues of the $j = -1$ sector:

$$\begin{aligned}
|4; +1, 1\rangle &= b_{0\uparrow}^\dagger b_{1\uparrow}^\dagger b_{-1\downarrow}^\dagger b_{1\downarrow}^\dagger |0\rangle \\
|4; +1, 2\rangle &= b_{-1\uparrow}^\dagger b_{1\uparrow}^\dagger b_{0\downarrow}^\dagger b_{1\downarrow}^\dagger |0\rangle, \\
|4; +1, 3\rangle &= b_{0\uparrow}^\dagger b_{-1\uparrow}^\dagger b_{0\downarrow}^\dagger b_{-1\downarrow}^\dagger |0\rangle, \\
|4; +1, 4\rangle &= b_{0\uparrow}^\dagger b_{-1\uparrow}^\dagger b_{1\uparrow}^\dagger b_{0\downarrow}^\dagger |0\rangle, \\
|4; +1, 5\rangle &= b_{-1\uparrow}^\dagger b_{0\downarrow}^\dagger b_{-1\downarrow}^\dagger b_{1\downarrow}^\dagger |0\rangle.
\end{aligned} \tag{39}$$

Thus one immediately sees that $H(4; j = +1) = H(4; j = -1)$. Hence, there is a double degeneracy of the eigenvalues $E_i(4; j = +1) = E_i(4; j = -1)$.

For $\lambda = 0$, the ground state is three-fold degenerate corresponding to the $S = 1$ triplet combination of the two unpaired spins in the cluster. These lowest three degenerate states correspond to $j = 0, \pm 1$. From the above analysis we conclude that isolated clusters with four electrons can be described through the effective hamiltonian

$$H_m = D(S_m^z)^2, \tag{40}$$

where S_m^z is the z -component of the pseudospin-1 operator acting on the spin-orbital space. D denotes the trigonal splitting induced by λ_{xy} and λ_z , and is an increasing function of SMOc as discussed in the main text.

C. Isolated triangular clusters with three electrons

The basis for $N = 3$ electrons consists of 20 configurations: 18 configurations with $S_z = 1/2$ ($N_\uparrow = 2, N_\downarrow = 1$)

or $S_z = -1/2$ ($N_\uparrow = 1, N_\downarrow = 2$) and 2 configurations with $S_z = 3/2$ ($N_\uparrow = 3, N_\downarrow = 0$) or $S_z = -3/2$ ($N_\uparrow = 0, N_\downarrow = 3$). The only allowed j values for the cluster with $N = 3$ electrons are $j = \pm \frac{1}{2}, +\frac{3}{2}$ with the largest (8×8) matrix corresponding to $j = +\frac{3}{2}$. The $j = -\frac{3}{2}$ sector is not given here since the configurations are just the same as the ones in the $j = +\frac{3}{2}$ sector.

1. $j = +3/2$

The configurations with $j = 3/2$ are

$$\begin{aligned}
|3; +3/2, 1\rangle &= b_{0\uparrow}^\dagger b_{1\uparrow}^\dagger b_{0\downarrow}^\dagger |0\rangle \\
|3; +3/2, 2\rangle &= b_{0\uparrow}^\dagger b_{-1\uparrow}^\dagger b_{-1\downarrow}^\dagger |0\rangle \\
|3; +3/2, 3\rangle &= b_{-1\uparrow}^\dagger b_{1\uparrow}^\dagger b_{1\downarrow}^\dagger |0\rangle \\
|3; +3/2, 4\rangle &= b_{1\uparrow}^\dagger b_{0\downarrow}^\dagger b_{1\downarrow}^\dagger |0\rangle \\
|3; +3/2, 5\rangle &= b_{0\uparrow}^\dagger b_{-1\uparrow}^\dagger b_{1\uparrow}^\dagger |0\rangle \\
|3; +3/2, 6\rangle &= b_{0\uparrow}^\dagger b_{0\downarrow}^\dagger b_{-1\downarrow}^\dagger |0\rangle \\
|3; +3/2, 7\rangle &= b_{-1\uparrow}^\dagger b_{-1\downarrow}^\dagger b_{1\downarrow}^\dagger |0\rangle \\
|3; +3/2, 8\rangle &= b_{0\downarrow}^\dagger b_{-1\downarrow}^\dagger b_{1\downarrow}^\dagger |0\rangle.
\end{aligned} \tag{41}$$

Yielding the 8×8 Hamiltonian matrix

$H(3; 3/2) =$

$$\begin{bmatrix} -3t_c + \frac{2U-5J_F/2}{3} + \frac{\lambda_z}{2} & \frac{U+J_F}{3} & \frac{U+J_F}{3} & -\frac{\lambda_{xy}}{\sqrt{2}} & -\frac{\lambda_{xy}}{\sqrt{2}} & 0 & 0 & 0 \\ \frac{U+J_F}{3} & \frac{2U-5J_F/2}{3} & -\frac{U+J_F}{3} & 0 & 0 & \frac{\lambda_{xy}}{\sqrt{2}} & -\frac{\lambda_{xy}}{\sqrt{2}} & 0 \\ \frac{U+J_F}{3} & -\frac{U+J_F}{3} & 3t_c + \frac{2U-5J_F/2}{3} - \frac{\lambda_z}{2} & -\frac{\lambda_{xy}}{\sqrt{2}} & -\frac{\lambda_{xy}}{\sqrt{2}} & 0 & 0 & 0 \\ -\frac{\lambda_{xy}}{\sqrt{2}} & 0 & -\frac{\lambda_{xy}}{\sqrt{2}} & \frac{2U-5J_F/2}{3} & 0 & \frac{U+J_F}{3} & \frac{U+J_F}{3} & 0 \\ -\frac{\lambda_{xy}}{\sqrt{2}} & 0 & -\frac{\lambda_{xy}}{\sqrt{2}} & 0 & 0 & 0 & 0 & 0 \\ 0 & \frac{\lambda_{xy}}{\sqrt{2}} & 0 & \frac{U+J_F}{3} & 0 & -3t_c + \frac{2U-5J_F/2}{3} + \frac{\lambda_z}{2} & -\frac{U+J_F}{3} & -\frac{\lambda_{xy}}{\sqrt{2}} \\ 0 & -\frac{\lambda_{xy}}{\sqrt{2}} & 0 & \frac{U+J_F}{3} & 0 & -\frac{U+J_F}{3} & 3t_c + \frac{2U-5J_F/2}{3} - \frac{\lambda_z}{2} & \frac{\lambda_{xy}}{\sqrt{2}} \\ 0 & 0 & 0 & 0 & 0 & -\frac{\lambda_{xy}}{\sqrt{2}} & \frac{\lambda_{xy}}{\sqrt{2}} & 0 \end{bmatrix} \quad (42)$$

2. $j = \pm 1/2$

and analogously for $j = -1/2$. The 6×6 hamiltonian matrix reads

We take the basis

$$\begin{aligned} |3; +1/2, 1\rangle &= b_{0\uparrow}^\dagger b_{0\downarrow}^\dagger b_{1\downarrow}^\dagger |0\rangle \\ |3; +1/2, 2\rangle &= b_{1\uparrow}^\dagger b_{-1\downarrow}^\dagger b_{1\downarrow}^\dagger |0\rangle \\ |3; +1/2, 3\rangle &= b_{-1\uparrow}^\dagger b_{0\downarrow}^\dagger b_{-1\downarrow}^\dagger |0\rangle \\ |3; +1/2, 4\rangle &= b_{-1\uparrow}^\dagger b_{1\uparrow}^\dagger b_{0\downarrow}^\dagger |0\rangle \\ |3; +1/2, 5\rangle &= b_{0\uparrow}^\dagger b_{1\uparrow}^\dagger b_{-1\downarrow}^\dagger |0\rangle \\ |3; +1/2, 6\rangle &= b_{0\uparrow}^\dagger b_{-1\uparrow}^\dagger b_{1\downarrow}^\dagger |0\rangle \end{aligned} \quad (43)$$

$$H(3; j = +1/2) = \begin{bmatrix} -3t_c + \frac{2U}{3} - \frac{5J_F}{6} - \frac{\lambda_z}{2} & \frac{U+J_F}{3} & \frac{U+J_F}{3} & 0 & 0 & \frac{\lambda_{xy}}{\sqrt{2}} \\ \frac{U+J_F}{3} & 3t_c + \frac{2U}{3} - \frac{5J_F}{6} + \frac{\lambda_z}{2} & -\frac{U+J_F}{3} & 0 & -\frac{\lambda_{xy}}{\sqrt{2}} & 0 \\ \frac{U+J_F}{3} & -\frac{U+J_F}{3} & \frac{2U}{3} - \frac{5J_F}{6} & 0 & 0 & 0 \\ 0 & 0 & 0 & \frac{2U}{3} - \frac{J_F}{3} & \frac{U-J_F/2}{3} & -\frac{U-J_F/2}{3} \\ 0 & -\frac{\lambda_{xy}}{\sqrt{2}} & 0 & \frac{U-J_F/2}{3} & \frac{2U}{3} - \frac{J_F}{3} + \lambda_z & \frac{U-J_F/2}{3} \\ \frac{\lambda_{xy}}{\sqrt{2}} & 0 & 0 & -\frac{U-J_F/2}{3} & \frac{U-J_F/2}{3} & \frac{2U}{3} - \frac{J_F}{3} - \lambda_z \end{bmatrix}$$

Due to Kramers theorem the eigenstates, $E_n(3; j = 1/2) = E_n(3; j = -1/2)$ and the energy levels for $E_n(3; j = 3/2)$ are at least doubly degenerate. With no SMOC present, $E_n(3; j = \pm 1/2) = E_n(3; j = 3/2)$ and

the eigenstates are four-fold degenerate. However, when SMOC is present $E_n(3; j = \pm 1/2) \neq E_n(3; j = 3/2)$ and the four-fold degeneracy is broken leading to two-fold degenerate levels.

¹ W. Witczak-Krempa, G. Chen, Y. Baek Kim, L. Balents, Ann. Rev. Cond. Mat. Phys., **5**, 57 (2014).

² D. Pesin and L. Balents, Nat. Phys. **6**, 376 (2010).

³ Z. Nussinov and J. van den Brink, Rev. Mod. Phys. **87**, 1 (2015).

⁴ G. Jackeli and G. Khaliullin, Phys. Rev. Lett. **102**, 017205 (2009).

⁵ N. B. Perkins, Y. Sizyuk, and P. Wölfle, Phys. Rev. B **89**, 035143 (2014).

⁶ Y. Sizyuk, C. Price, P. Wölfle, and N. B. Perkins, Phys. Rev. B **90**, 155126 (2014).

⁷ M. G. Yamada, H. Fujita, M. Oshikawa, arXiv:1605.04471.

⁸ A. Kitaev, Ann. Phys. **321**, 2 (2006).

⁹ A. Khosla, A. C. Jacko, J. Merino, and B. J. Powell, Phys. Rev. B **95**, 115109 (2017).

¹⁰ A. C. Jacko, A. Khosla, J. Merino, and B. J. Powell, arXiv:1612.02929.

¹¹ J. Merino, A. C. Jacko, A. L. Khosla, and B. J. Powell, Phys. Rev. B **94**, 205109 (2016).

¹² A. C. Jacko, C. Janani, K. Koepernik, and B. J. Powell, Phys. Rev. B **91**, 125140 (2015).

¹³ A. Ruegg, J. Wen, and G. A. Fiete, Phys. Rev. B **81**,

- 205115 (2010).
- ¹⁴ C. Kane and E. Z. Mele, Phys. Rev. Lett. **95**, 146802 (2005).
 - ¹⁵ H. Yao and S. A. Kivelson, Phys. Rev. Lett. **99**, 247203 (2007).
 - ¹⁶ B. J. Powell, J. Merino, A. L. Khosla, A. C. Jacko, arXiv:1612.04926.
 - ¹⁷ C. Janani, J. Merino, I. P. McCulloch, and B. J. Powell, Phys. Rev. Lett. **113**, 267204 (2014).
 - ¹⁸ C. Janani, J. Merino, I. P. McCulloch, and B. J. Powell, Phys. Rev. B **90**, 035120 (2014).
 - ¹⁹ B. J. Powell, Coord. Chem. Rev. **295**, 46 (2015).
 - ²⁰ T. Yildirim, A. B. Harris, A. Aharony, and O. Entin-Wohlman, Phys. Rev. B **52**, 10239 (1995).
 - ²¹ T. Moriya, Phys. Rev. **120**, 91 (1960).
 - ²² H. L. Nourse, I. P. McCulloch, C. Janani, and B. J. Powell, Phys. Rev. B **94**, 214418 (2016).
 - ²³ A. B. Harris and R. V. Lange Phys. Rev. **157**, 29 (1967).
 - ²⁴ K. A. Chao, J. Spalek, and A M Oleś, J. Phys. C **10**, L271 (1977).
 - ²⁵ I. Affleck, T. Kennedy, E. H. Lieb, and H. Tasaki, Phys. Rev. Lett. **59**, 799 (1987).
 - ²⁶ S. R. White and D. A. Huse, Phys. Rev. B **48**, 3844 (1993).
 - ²⁷ F. D. M. Haldane, Phys. Lett. A **93**, 464 (1983).
 - ²⁸ F. D. M. Haldane, Phys. Rev. Lett. **50**, 1153 (1983).
 - ²⁹ G. Gomez-Santos, Phys. Rev. Lett. **63**, 790 (1989).
 - ³⁰ F. Pollmann, E. Berg, A. M. Turner, M. Oshikawa, Phys. Rev. B **85**, 075125 (2012).
 - ³¹ A. F. Albuquerque, C. J. Hamer, and J. Oitmaa, Phys. Rev. B **79**, 4412 (1989).
 - ³² S. Hu, B. Normand, X. Wang, L. Yu, Phys. Rev. B **84**, 220402(R), (2011).
 - ³³ A. Langari, F. Pollmann, and M. Siahatgar, J. Phys. Cond. Matt. **25**, 406002 (2013).
 - ³⁴ Y.-C. Tzeng and M.-F. Yang, Phys. Rev. A **77**, 012311 (2008).
 - ³⁵ K. Wierschem and P. Sengupta, JPS Conf. Proc. **3**, 012005 (2014).
 - ³⁶ T. Sakai and M. Takahashi, Phys. Rev. B **42**, 4537 (1990).
 - ³⁷ I. Affleck, Phys. Rev. B **41**, 6697 (1990).
 - ³⁸ E. Orignac, R. Citro, and T. Giamarchi, Phys. Rev. B **75**, 140403 (2007).
 - ³⁹ A. K. Bera, B. Lake, A. T. M. N. Islam and A. Schneidewind, Phys. Rev. B **92**, 060412 R (2015).
 - ⁴⁰ M. Dupont, S. Capponi, and N. Laflorencie, Phys. Rev. B **94**, 144409 (2016).
 - ⁴¹ S. H. Chun, *et. al.*, Nat. Phys. **11**, 462 (2015).
 - ⁴² S.-S. Gong, W. Zhu, and D. N. Sheng, Phys. Rev. B **92**, 195110 (2015).
 - ⁴³ O. Cepas, C. M. Fong, P. W. Leung, and C. Lhuillier, Phys. Rev. B **78**, 140405(R) (2008).
 - ⁴⁴ L. Messio, S. Bieri, C. Lhuillier, and B. Bernu, arXiv: 1701.01243.